# Solute trapping in rapid solidification of a binary dilute system: A phase-field study

P. K. Galenko*
*Institut für Materialphysik im Weltraum, Deutsches Zentrum für Luft- und Raumfahrt (DLR), D-51170 Köln, Germany and Institut für Festkörperphysik, Ruhr-Universität Bochum, D-44780 Bochum, Germany*

E. V. Abramova
*Institut für Materialphysik im Weltraum, Deutsches Zentrum für Luft- und Raumfahrt (DLR), D-51170 Köln, Germany and ICAMS, Ruhr-Universität Bochum, D-44780 Bochum, Germany*

D. Jou
*Departament de Física, Universitat Autònoma de Barcelona, E-08193 Bellaterra, Catalonia, Spain*

D. A. Danilov and V. G. Lebedev
*Department of Theoretical Physics, Udmurt State University, 426034 Izhevsk, Russia*

D. M. Herlach
*Institut für Materialphysik im Weltraum, Deutsches Zentrum für Luft- und Raumfahrt (DLR), D-51170 Köln, Germany*

(Received 10 May 2011; revised manuscript received 21 September 2011; published 31 October 2011)

The phase-field model of Echebarria, Folch, Karma, and Plapp [Phys. Rev. E **70**, 061604 (2004)] is extended to the case of rapid solidification in which local nonequilibrium phenomena occur in the bulk phases and within the diffuse solid-liquid interface. Such an extension leads to the fully hyperbolic system of equations given by the atomic diffusion equation and the phase-field equation of motion. This model is applied to the problem of solute trapping, which is accompanied by the entrapment of solute atoms beyond chemical equilibrium by a rapidly moving interface. The model predicts the beginning of complete solute trapping and diffusionless solidification at a finite solidification velocity equal to the diffusion speed in bulk liquid.

DOI: 10.1103/PhysRevE.84.041143 PACS number(s): 05.70.Ln, 05.70.Fh, 64.60.My

## I. INTRODUCTION

The term "solute trapping" has been introduced to describe the process of nonequilibrium solute redistribution at the solid-liquid interface, which is accompanied by the entrapment of solute away from chemical equilibrium in solidification [1–3]. This process results in the deviation of the partition coefficient for solute distribution at the interface toward unity away from its equilibrium value, independently of the sign of the chemical potential [4].

The effect of solute trapping has been investigated theoretically using semisharp-interface models based on the continuous growth model [3,4] as well as using phase-field models [5–9] of rapid solidification. In particular, solute trapping is characterized by the solute segregation coefficient $k(V)$, which is dependent on the interface velocity $V$, and is evaluated by the following ratio:

$$k(V) = \left.\frac{\text{concentration in solid}}{\text{concentration in liquid}}\right|_{\text{interface}}. \qquad (1)$$

This segregation coefficient $k(V)$ includes the kinetic parameter in a form of the solute diffusion speed $V_D^I$ at the interface [3,4]. Quantitative analysis of $k(V)$ shows reasonable agreement with experimental findings at small and moderate growth velocities of crystals. However, the results of natural experiments exhibit a complete solute trapping regime which occurs at $k(V) = 1$ with a finite interface velocity $V$, which is not predicted by the function $k(V)$ including the solute diffusion speed $V_D^I$ at the interface only. As it has been analytically derived [10] and numerically simulated [11], to describe increasing $k(V)$ up to $k(V) = 1$ at a finite interface velocity $V$ the model has to include both the finite speed $V_D^I$ at the interface and the finite speed $V_D^B$ of atomic diffusion in bulk phases.

The main scope of the present paper is to develop a phase-field model for solute trapping in rapid solidification which takes into account both solute diffusion speeds within the diffuse interface and bulk phases. Rapid solidification is initiated by the large difference of free energy between the stable solid and metastable liquid that in general occurs when a system is undercooled far below liquidus temperature [12]. These conditions lead to rapid motion of the solid-liquid interface with a velocity comparable to the speed of atomic diffusion. The movement of a solidification front at such fast velocities can lead to bulk phases that are not in a local chemical equilibrium and both speeds in the bulk and at the interface should be taken into account. As shown [10], and recently verified in atomistic simulations [13], the trapping of solutal atoms during rapid solidification cannot be described by purely parabolic models of diffusion. Therefore we develop the hyperbolic model which takes these two diffusion speeds into account. This development is given as an extension of the Echebarria-Folch-Karma-Plapp phase-field model (the EFKP model) as is described in the original work [14] and is summarized in Appendixes A 1 and A 2. The EFKP-model was

*peter.galenko@dlr.de

 

previously developed for the case of diluted binary systems solidifying close to thermodynamic equilibrium. The present extension of the EFKP model to the hyperbolic case leads to a model represented by a couple of partial differential equations of hyperbolic type. To predict the complete solute trapping observed in experiments and predicted by the sharp-interface model (see results and discussions in Refs. [10–12]), the fully hyperbolic model is analyzed, and the results compared with those of the parabolic phase-field model [14].

The paper is organized as follows. A phase-field model is formulated in Sec. II. Equilibrium and dynamical features of the model are presented in Sec. III. Governing equations and parameters of the model in one spatial dimension for the diffuse interface moving with constant velocity are given in Sec. IV. The method of numerical solution of equations and the special definition of the solute segregation function are then described in Sec. V. Numerical results obtained for concentration profiles, solute segregation, and kinetic phase diagrams are discussed in Sec. VI. A summary of the conclusions is presented in Sec. VII. Finally, in Appendixes A, B, and C we summarize analytical results on phase-field models described by parabolic and hyperbolic equations.

## II. MODEL

A condition of solute trapping by moving diffuse interface in a rapidly solidifying system can be formulated as follows. During rapid solidification the solute trapping effect takes place when a solute has not enough time to escape the advancing diffuse interface and accumulates in it. This effect becomes important at interface velocities $V$ higher than a characteristic value of the order of $V_c \sim D/\delta$ (with $D$ being characteristic diffusion coefficient of a solute and $\delta$ the interface thickness). Indeed, when $V > V_c$, the characteristic time $\delta/V$ of advance of one interface thickness $\delta$ becomes smaller than the time $\delta^2/D$ which the solute takes to diffuse through the interface. As a result of these definitions, the solute trapping by diffuse interface exists by the following velocity condition:

$$V > D/\delta,$$

or by the following time scale condition:

$$\delta/V < \delta^2/D.$$

From these conditions follows that the critical velocity for the beginning of solute trapping becomes smaller as the interfacial thickness increases. Therefore in solidifying systems with thicker phase interface the solute trapping is more pronounced.

To analyze the solute trapping during rapid solidification, consider a binary system consisting of $A$ atoms (solvent) together with a tiny amount of $B$ atoms (solute) under constant temperature $T$ and constant pressure. The requirement that the free energy monotonically decreases during the relaxation of the entire system to equilibrium leads to the following equations [15]:

$$\tau_D \frac{\partial^2 C}{\partial t^2} + \frac{\partial C}{\partial t} = \vec{\nabla} \cdot \left[ M_C \left( \frac{\partial^2 f}{\partial C^2} \vec{\nabla} C + \frac{\partial^2 f}{\partial C \partial \varphi} \vec{\nabla} \varphi \right) \right], \quad (2)$$

$$\tau_\varphi \frac{\partial^2 \varphi}{\partial t^2} + \frac{\partial \varphi}{\partial t} = M_\varphi \left( \varepsilon_\varphi^2 \nabla^2 \varphi - \frac{\partial f}{\partial \varphi} \right), \quad (3)$$

where $f$ is the free energy density, $C$ is the solute concentration (of $B$ atoms), $\tau_D$ is the relaxation time for the diffusion flux, $M_C$ is the mobility of $B$ atoms, $\tau_\varphi$ is the time scale for the relaxation of the rate of change of the phase field $\partial\varphi/\partial t$, and $M_\varphi$ is the mobility of the phase field.

Equations (2) and (3) represent a fully hyperbolic system of equations. It describes solidifying system in which the free energy does not increase in time [16] and the atomic balance law is satisfied with the assumption of positive values of the mobility coefficients $M_C$ and $M_\varphi$.

To complete the definition of the system (2) and (3), let us choose an explicit free energy density $f$ under condition of local equilibrium. Following the EFKP model, the local equilibrium free energy density $f$ is chosen as the ideal solution of a dilute binary system [14]:

$$f(C,\varphi) = f^A(T_A) - (T - T_A)s(\varphi) + \epsilon(\varphi)C + \frac{RT}{v_m}(C \ln C - C) + W g(\varphi), \quad (4)$$

where $f^A(T)$ is the free energy density of a pure system consisting of a solvent (pure $A$ atoms), $T_A$ is the solidification temperature of the solvent, $R$ is the gas constant, $v_m$ is the molar volume (assumed equal for $A$ and $B$ atoms), $W$ is the height of the energetic barrier, which is modeled by the double-well function

$$g(\varphi) = \varphi^2(1-\varphi)^2. \quad (5)$$

The entropy density $s(\varphi)$ and the internal energy density $\epsilon(\varphi)$ are derived using the dilute alloy approximation (see Ref. [14])

$$s(\varphi) = \frac{s_s + s_l}{2} - p_s(\varphi)\frac{L}{2T_A}, \quad p_s(\varphi) = 1 - 2p(\varphi), \quad (6)$$

$$\epsilon(\varphi) = \frac{\epsilon_s + \epsilon_l}{2} - p_\epsilon(\varphi)\frac{RT}{2v_m}\ln k_e,$$
$$p_\epsilon(\varphi) = \frac{2}{\ln k_e}\ln[k_e + p(\varphi)(1-k_e)] - 1, \quad (7)$$

where $L$ is the latent heat of solidification, $k_e$ is the equilibrium solute partition coefficient, and indexes $l$ and $s$ are related to the liquid and solid phase, respectively.

The interpolation function $p(\varphi)$ is taken to be

$$p(\varphi) = \varphi^2(3 - 2\varphi), \quad (8)$$

with

$$1 - p(\varphi) = p(1-\varphi),$$
$$\left.\frac{dp(\varphi)}{d\varphi}\right|_{\varphi=0} = \left.\frac{dp(\varphi)}{d\varphi}\right|_{\varphi=1} = 0. \quad (9)$$

The functions $g(\varphi)$ and $p(\varphi)$ [given by Eqs. (5) and (8), respectively] are a feature of the specific choice of phase-field model used here, which is described in Refs. [7,17]. These functions define the liquid state for $\varphi = 1$ and the solid state for $\varphi = 0$.

## III. EQUILIBRIUM AND DYNAMICS

### A. Features of the equilibrium state

#### 1. Phase stability

The stability of the system given by the free energy minimum at equilibrium is defined by the sufficient condition $\partial^2 f/\partial\varphi^2 > 0$. Taking Eqs. (4)–(8) into account, this condition is obtained as

$$\frac{\partial^2 f}{\partial\varphi^2} = \frac{RT}{v_m}\left[\frac{(1-k_e)^2 C}{[k_e+(1-k_e)p(\varphi)]^2}6\sqrt{g(\varphi)} - \left(\frac{T_A-T}{T_A}\frac{Lv_m}{RT}+\frac{(1-k_e)C}{k_e+(1-k_e)p(\varphi)}\right)6\frac{d\sqrt{g(\varphi)}}{d\varphi} + \frac{Wv_m}{RT}\frac{d^2 g(\varphi)}{d\varphi^2}\right]. \quad (10)$$

Analysis shows that Eq. (10) is strictly positive at equilibrium $T \to T_A$ in phases ($\varphi = 0$ and $\varphi = 1$). This gives sufficient thermodynamical stability, $\partial^2 f/\partial\varphi^2 > 0$, corresponding to coexistence of both phases at equilibrium. Also, due to equality between second-order crossed derivatives $\partial^2 f/\partial C\partial\varphi$ and $\partial^2 f/\partial\varphi\partial C$, and using Eqs. (5)–(8) one gets

$$\frac{\partial^2 f}{\partial C\partial\varphi} = \frac{\partial^2 f}{\partial\varphi\partial C} = -\frac{RT}{v_m}\cdot\frac{6\sqrt{g(\varphi)}(1-k_e)}{k_e+(1-k_e)p(\varphi)}. \quad (11)$$

This equality is used below: it has zero value in phases ($\varphi = 1$ or $\varphi = 0$) and it is negative within the diffuse interface ($0 < \varphi < 1$).

#### 2. Equilibrium phase-field profiles

Equilibrium profile of the phase field can be obtained from solution of the equation

$$\varepsilon_\varphi^2\nabla^2\varphi - \frac{\partial f}{\partial\varphi} = 0,$$

following naturally from Eq. (3). This solution can be illustrated in two models (taken for simplicity in one spatial dimension): the EFKP model in which the free energy density (4) gives the equation (see Appendix A 2)

$$\varepsilon_\varphi^2\frac{d^2\varphi}{dx^2} - W\frac{dg(\varphi)}{d\varphi} = -\frac{RT}{2v_m}C_l\left[(1-k_e)\frac{dp_s(\varphi)}{d\varphi}+\ln k_e\frac{C_0(x)}{C_l}\frac{dp_\epsilon(\varphi)}{d\varphi}\right]\equiv 0, \quad (12)$$

and the Wheeler, Boettinger, and McFadden model (WBM model [5,7]) in which the free energy density (A24)–(A26) leads to the equation (see Appendix A 3)

$$\frac{d^2\varphi}{dx^2} - \frac{9}{2}\frac{dg(\varphi)}{d\varphi} = \frac{1}{2}\frac{\delta}{d_0}\frac{T}{T_A}C_l[1-k_e+\ln(k_e)e^{\ln k_e[1-p(\varphi)]}]\frac{dp(\varphi)}{d\varphi}, \quad (13)$$

where $C(x)$ and $C_l$ are the equilibrium concentration profile and the liquid concentration, respectively, and the ratio $\delta/d_0$ is given by the parameters defined below by Eq. (36).

The EFKP model predicts the equilibrium state in such a manner that the right hand side of Eq. (12) has zero value.

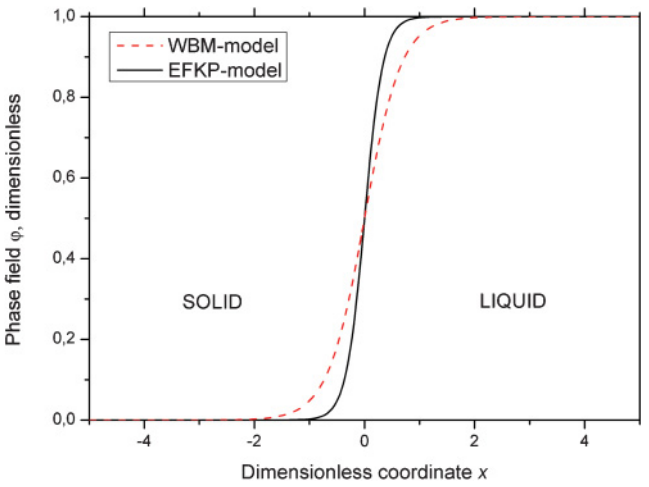


FIG. 1. (Color online) Equilibrium profiles of the phase field $\varphi$ predicted by WBM model, Eq. (13), and EFKP model, Eq. (14).

This feature of EFKP model gives a simple kink solution (see Appendix A 2)

$$\varphi = \frac{1}{2}+\frac{1}{2}\tanh\left(\frac{\sqrt{W}x}{\sqrt{2}\varepsilon_\varphi}\right). \quad (14)$$

Note, however, that the right hand side of Eq. (13) does not vanish in equilibrium predicted by the WBM model (see Appendix A 3). This gives a more diffuse profile of $\varphi$ obtained from the WBM model in comparison with the steeper profile of $\varphi$ obtained from the EFKP model. It is clearly shown in Fig. 1. Such difference in the equilibrium profiles of $\varphi$ affects, obviously, the concentration profiles and values of solute segregation coefficients not only in equilibrium but also in dynamics. Note finally that the critical analysis of the WBM model also was presented for equilibrium and near equilibrium conditions within the context of multiphase-field models [18].

### B. Solute diffusion dynamics

To treat the dynamics of rapid solidification we use the semihyperbolic phase-field model of solidification [19] in which the diffusion field is described by the hyperbolic equation and phase-field dynamics is given by the parabolic equation [20]. To do this, we generalize the set of thermodynamic variables for free energy (4) such that it includes a contribution from the diffuse interface energy $\propto\nabla^2\varphi$ and a pure nonequilibrium contribution $\propto J^2$. Then, using the entropy representation of nonequilibrium states in fast transitions [15],

$$S(C,\varphi,\vec{\nabla}\varphi,\vec{J}) = -\frac{1}{T}f(C,\varphi) - \frac{1}{2}\varepsilon_\varphi^2|\nabla\varphi|^2 - \frac{1}{2}\alpha\vec{J}\cdot\vec{J},$$

with the coefficient $\alpha = \tau_D/(TD^*)$, the Gibbs equation is described by

$$dS(C,\varphi,\vec{\nabla}\varphi,\vec{J}) = -\frac{\mu(C,\varphi)}{T}dC - \frac{\eta(C,\varphi)}{T}d\varphi + \varepsilon_\varphi^2\nabla^2\varphi d\varphi - \frac{\tau_D}{TD^*}\vec{J}\cdot d\vec{J}, \quad (15)$$

where $\tau_D$ is the relaxation time of flux $\vec{J}$ to local equilibrium steady state and

$$D^*(\varphi,C) = (\partial\mu/\partial C)^{-1} D(\varphi) \tag{16}$$

is the diffusion coefficient. As compared to Eq. (4), the chemical potential $\mu$ and the function $\eta$ from Eq. (15) are defined by

$$\begin{aligned}\mu(C,\varphi) &= -T\frac{\partial S}{\partial C} = \epsilon(\varphi) + \frac{RT}{v_m}\ln C,\\ \eta(C,\varphi) &= -T\frac{\partial S}{\partial \varphi} = (T_A - T)\frac{ds(\varphi)}{d\varphi}\\ &\quad + C\frac{d\epsilon(\varphi)}{d\varphi} + W\frac{dg(\varphi)}{d\varphi}.\end{aligned} \tag{17}$$

With Eq. (17), we arrive at the condition

$$\frac{\partial \eta}{\partial C} = \frac{\partial \mu}{\partial \varphi}, \tag{18}$$

which is equivalent to Eq. (11). The third term on the right hand side of Eq. (15) is responsible for space nonlocality in $\varphi$. Its existence is due to large spatial gradients of $\varphi$ within the diffuse interface. The form of the last term in Eq. (15) is known from extended thermodynamics [21] and from the other nonequilibrium phenomenology, for instance, from the general equation for the nonequilibrium reversible-irreversible coupling (GENERIC) formalism [22]: it appears due to relaxation of the flux $\vec{J}$ to its steady-state value with the characteristic time $\tau_D$. The function $D^*$ defined by Eq. (16) is related to the diffusion coefficient $D(\varphi)$ within the diffusive interface through the diffusion coefficient of $B$ atoms dissolved in $A$ solvent within the diffuse interface taking into account bulk diffusion coefficients $D_L$ and $D_S$ in the liquid and solid, respectively, as follows:

$$D(\varphi) = D_S + p(\varphi)(D_L - D_S). \tag{19}$$

To qualitatively evaluate the dynamics, we obtain the evolution equation for the flux coupled with the phase field. The mass balance has the following form:

$$\frac{\partial C}{\partial t} = -\vec{\nabla}\cdot\vec{J}, \tag{20}$$

and the entropy balance reads as

$$\frac{\partial S}{\partial t} + \vec{\nabla}\cdot\vec{J}_S = \sigma, \tag{21}$$

where $\vec{J}_S$ is the entropy flux, and $\sigma$ is the entropy production. Obeying the restrictions of the second law of thermodynamics, the time derivative of Eq. (15) is described by

$$\begin{aligned}\frac{\partial S}{\partial t} &= \vec{\nabla}\cdot\left[\frac{\mu}{T}\vec{J}\right] - \frac{1}{T}\left[\left(\vec{\nabla}\mu + \frac{\tau_D}{D}\frac{\partial \vec{J}}{\partial t}\right)\cdot\vec{J}\right.\\ &\quad \left. + \left(\eta - \tilde{\varepsilon}_\varphi^2\nabla^2\varphi\right)\frac{\partial\varphi}{\partial t}\right],\end{aligned} \tag{22}$$

where $\tilde{\varepsilon}_\varphi^2 = T\varepsilon_\varphi^2$ is the temperature dependent gradient energy factor, and Eq. (20) has been used.

Now, using the structure of Eq. (22), we obtain the flux and production of entropy in such a way that the coupling between $\varphi$ and $C$ will be explicitly revealed. First, we write the entropy flux as

$$\vec{J}_S = -\frac{\mu}{T}\vec{J} - \frac{\beta_0\eta}{T}\vec{J}. \tag{23}$$

Second, taking the structure of Eq. (22) into account, we find the entropy production from the balance (21) as follows:

$$\begin{aligned}\sigma &= -\frac{\vec{J}}{T}\cdot\left[\vec{\nabla}\mu + \frac{\tau_D}{D^*}\frac{\partial\vec{J}}{\partial t} + \beta_0\vec{\nabla}\eta\right]\\ &\quad - \frac{1}{T}\frac{\partial\varphi}{\partial t}\left[\eta - \tilde{\varepsilon}_\varphi^2\nabla^2\varphi + \beta_0\eta\vec{\nabla}\cdot\vec{J}\right] \geqslant 0.\end{aligned} \tag{24}$$

The terms $\propto \beta_0\eta\vec{J}$ and $\propto \beta_0\eta\vec{\nabla}\cdot\vec{J}$ in Eqs. (23) and (24) are nonlocal contributions vanishing at equilibrium and $\beta_0$ is a coefficient providing nonlocal coupling between $\varphi$ and $C$ by analogy with analysis of other coupled phenomena [21]. We choose the *positive sign of* $\beta_0$ in such a way that this coupling has led to the increase of entropy production and to accelerate approaching toward equilibrium in solidification. Indeed, the function

$$\begin{aligned}\eta(\varphi) &= \frac{RT}{v_m}\left\{6\sqrt{g(\varphi)}\left[\frac{T_A - T}{T_A T}\cdot\frac{L}{(R/v_m)}\right.\right.\\ &\quad \left.\left. - \frac{(1-k_e)C}{k_e + (1-k_e)p(\varphi)}\right] + \frac{Wv_m}{RT}\frac{dg(\varphi)}{d\varphi}\right\}\end{aligned} \tag{25}$$

from Eq. (17) is always positive, $\eta(\varphi) > 0$, at the part of diffuse interface $0 < \varphi < 1/2$ adjacent to the solid phase where $\nabla\cdot\vec{J} < 0$. Also, we have $\eta(\varphi) < 0$ at the part of diffuse interface $1/2 < \varphi < 1$ adjacent to the liquid phase where $\nabla\cdot\vec{J} > 0$. Then, the terms $\propto\beta_0\eta\vec{J}$ and $\propto\beta_0\eta\vec{\nabla}\cdot\vec{J}$ increase the entropy production (24) with the positive value of the coupling coefficient, $\beta_0 > 0$, which is used for the analysis below.

From the bilinear quadratic form (24) the relations between thermodynamic fluxes and their conjugated forces look like

$$\vec{J} = -L_1\left(\frac{\tau_D}{D^*}\frac{\partial\vec{J}}{\partial t} + \vec{\nabla}\mu + \beta_0\vec{\nabla}\eta\right), \tag{26}$$

$$\frac{\partial\varphi}{\partial t} = -L_2\left(\eta - \tilde{\varepsilon}_\varphi^2\nabla^2\varphi + \beta_0\vec{\nabla}\cdot\vec{J}\right). \tag{27}$$

Thus Eqs. (26) and (27) directly exhibit the coupling between the diffusion flux $\vec{J}$ and phase field $\varphi$ with positive phenomenological coefficients $L_1 > 0$ and $L_2 > 0$ providing a non-negative value for the entropy production in Eq. (24).

In Eq. (26), the coefficient $L_1$ may be identified as $D^*$, which leads to the following evolution equation for the solute diffusion flux:

$$\begin{aligned}\tau_D\frac{\partial\vec{J}}{\partial t} + \vec{J} &= -D^*\vec{\nabla}\mu(C,\varphi) - D^*\beta_0\vec{\nabla}\eta(C,\varphi)\\ &= -D^*\left[\frac{\partial\mu}{\partial C} + \beta_0\frac{\partial\eta}{\partial C}\right]\vec{\nabla}C\\ &\quad - D^*\left[\frac{\partial\mu}{\partial\varphi} + \beta_0\frac{\partial\eta}{\partial\varphi}\right]\vec{\nabla}\varphi.\end{aligned} \tag{28}$$

The coefficient $L_2$ in Eq. (27) is identified as the mobility of the phase field. However, just for the qualitative analysis of solute diffusion within the diffuse interface, we skip Eq. (27)

from the consideration and treat only Eq. (28) in this section. Namely, we analyze possible effects of solute trapping or solute rejection existing due to motion of the diffuse interface. Taking the diffusion coefficient (16) into account, Eq. (28) can be presented as

$$\tau_D \frac{\partial \vec{J}}{\partial t} + \vec{J} = \vec{J}_C + \vec{J}_\varphi, \tag{29}$$

where the contribution from the concentration gradient is given by

$$\vec{J}_C = -D(\varphi)\left[1 + \beta_0 \frac{\partial\eta/\partial C}{\partial\mu/\partial C}\right]\vec{\nabla} C, \tag{30}$$

the contribution from the phase-field gradient is presented as

$$\vec{J}_\varphi = \vec{J}_\varphi^{(1)} + \vec{J}_\varphi^{(2)}, \tag{31}$$

$$\vec{J}_\varphi^{(1)} = -D(\varphi)\frac{\partial\mu/\partial\varphi}{\partial\mu/\partial C}\vec{\nabla}\varphi, \tag{32}$$

$$\vec{J}_\varphi^{(2)} = -D(\varphi)\beta_0 \frac{\partial\eta/\partial\varphi}{\partial\mu/\partial C}\vec{\nabla}\varphi, \tag{33}$$

and the diffusion coefficient is given by Eq. (19). Using Eqs. (5)–(8), (17), and (18), derivatives from the flux contributions (30)–(33) are

$$\frac{\partial\eta/\partial C}{\partial\mu/\partial C} \equiv \frac{\partial\mu/\partial\varphi}{\partial\mu/\partial C} = -\frac{6(1-k_e)C\sqrt{g(\varphi)}}{k_e + p(\varphi)(1-k_e)}, \tag{34}$$

$$\begin{aligned}\frac{\partial\eta/\partial\varphi}{\partial\mu/\partial C} = C\Bigg\{ &\frac{(1-k_e)^2 C}{[k_e + (1-k_e)p(\varphi)]^2} 6\sqrt{g(\varphi)} \\ &- \left[\frac{T_A - T}{T_A}\frac{L v_m}{RT} + \frac{C(1-k_e)}{k_e + (1-k_e)p(\varphi)}\right] 6\frac{d\sqrt{g(\varphi)}}{d\varphi} \\ &+ \frac{W v_m}{RT}\frac{d^2 g(\varphi)}{d\varphi^2}\Bigg\} \equiv C\frac{\partial^2 f}{\partial\varphi^2}.\end{aligned} \tag{35}$$

As we noted, the coupling between fields of $C$ and $\varphi$ proceeds with the positive coefficient $\beta_0 > 0$ in Eqs. (26) and (27) that leads to an increase of the positive entropy production by Eq. (24) within the diffuse interface. From this follow the specific features of the solute diffusion dynamics within the diffuse interface.

(i) *Solute diffusion in the presence of the diffuse interface.* The function (34) reduces solute rejection by the flux $\vec{J}_C$ within the diffuse interface, Eq. (30), because $g(\varphi) > 0$ and $\beta_0 > 0$. Also, due to equality (18), the function (34) contributes to solute accumulation by $\vec{J}_\varphi^{(1)}$, Eq. (32), having the same sign as $\vec{\nabla}\varphi$ with $g(\varphi) > 0$. Therefore the flux $\vec{J}_\varphi^{(1)}$ contributes to decreased solute transport in the direction of the diffuse interface motion, i.e., in the direction toward increasing values of $\varphi$.

(ii) *Solute accumulation at the center of the diffuse interface.* The second contribution $\vec{J}_\varphi^{(2)}$, Eq. (33), is defined by Eq. (35). This term is positive in both phases and at the boundaries of the diffuse interface. However, it has a minimum with negative values around $\varphi = 1/2$. Therefore, with this term, the contribution of $\vec{J}_\varphi^{(2)}$ gives accumulation of the solute at $\varphi = 1/2$, i.e., at the center of the diffuse interface. Thus the contribution $\vec{J}_\varphi^{(2)} > 0$ at $\beta_0 > 0$ describes a solutal motion toward the center of the diffuse interface. This contributes to trapping, but not into the solid phase itself, but in the center of the diffuse interface, $\varphi = 1/2$.

## IV. MODEL PARAMETERS AND GOVERNING EQUATIONS

Here we summarize the main parameters and equations for the hyperbolic extension of the EFKP model. Note that the model parameters presented here can also be chosen for the WBM model [5,7] and for its hyperbolic extension [11].

### A. Parameters of the phase field and solute diffusion

The present computations use the following model parameters: the gradient energy factor $\varepsilon_\varphi^2$, the energetic barrier height $W$, the capillary parameter $d_0$, and the mobility $M_\varphi$ of the phase field expressed in terms of the surface energy $\sigma$, the interfacial width $\delta$, and the phase-field diffusion parameter $\nu$:

$$\begin{aligned}\varepsilon_\varphi^2 &= 2\sigma\delta, \quad W = \frac{9\sigma}{\delta}, \\ d_0 &= \frac{\sigma v_m}{RT_A}, \quad M_\varphi = \frac{\nu}{2\sigma\delta},\end{aligned} \tag{36}$$

the diffusion coefficient by Eq. (19), and the atomic mobility:

$$M_C(T, C, \varphi) = \left(\frac{\partial^2 f}{\partial C^2}\right)^{-1} D(\varphi). \tag{37}$$

Note that the phase-field mobility from Eq. (36) is assumed to be positive at the positive phase-field diffusivity $\nu > 0$ and the atomic mobility (37) is positive at $\partial^2 f/\partial C^2 > 0$. This guarantees monotonic behavior of the free energy with its nonpositive dissipation in a solidifying system.

In addition to the parameters, used usually for the systems evolving around equilibrium, the present problem of fast propagating interface includes four additional kinetic parameters as described in Appendix B and are given in Table I. The parameters lead to characteristic speeds for solute diffusion and interface propagation. They are defined by the thickness $\delta$ of the interface and relaxation times of the solute diffusion and phase fields to local equilibrium.

### B. Equations in the moving reference frame

The solute trapping problem is analyzed in one spatial dimension with a planar interface using the model parameters (36) and (37) and the values of Table I. In this case, we use the following dimensionless coordinate reference frame, $x \to (x - Vt)/\delta$ and $t \to t\nu/\delta^2$, which is moving with the constant

TABLE I. Analytical expressions for the characteristic speeds of atomic diffusion and phase-field propagation.

| Parameter | Expression |
|---|---|
| Speed of solute diffusion within the diffuse interface | $V_D^I = D_L/\delta$ |
| Scale of diffuse interface speed | $V_\varphi^I = \nu/\delta$ |
| Maximum speed of solute diffusion in bulk liquid | $V_D^B = (D_L/\tau_D)^{1/2}$ |
| Maximum speed for phase-field propagation | $V_\varphi^B = (\nu/\tau_\varphi)^{1/2}$ |

interface velocity $V$ with the origin $x = 0$ placed at $\varphi = 1/2$. Then, the governing equations (2) and (3) can be written in the following dimensionless form for the concentration field (see Appendix B 1):

$$\frac{V^2}{\left(V_D^B\right)^2}\frac{d^2C}{dx^2} - \frac{V}{V_D^I}\frac{dC}{dx} = \frac{d}{dx}\left(\hat{D}(\varphi)\frac{dC}{dx}\right) + \frac{d}{dx}\left(\hat{D}(\varphi)C\Theta(\varphi)\frac{dp(\varphi)}{d\varphi}\frac{d\varphi}{dx}\right), \quad (38)$$

and for the phase field (see Appendix B 2)

$$\frac{V^2}{\left(V_\varphi^B\right)^2}\frac{d^2\varphi}{dx^2} - \frac{V}{V_\varphi^I}\frac{d\varphi}{dx} = \frac{d^2\varphi}{dx^2} - \frac{9}{2}\frac{dg(\varphi)}{d\varphi} + \frac{1}{2}\frac{\delta}{d_0}\frac{T}{T_A}\Lambda(T,C,\varphi)\frac{dp(\varphi)}{d\varphi}. \quad (39)$$

Equations (38) and (39) describe quasistationary phase-field dynamics in which, using contributions (5)–(9) to the free energy density (4), the following functions are introduced:

$$\Theta(\varphi) = -\frac{1-k_e}{k_e + (1-k_e)p(\varphi)}, \quad (40)$$

$$\Lambda(T,C,\varphi) = \frac{(1-k_e)C}{k_e + (1-k_e)p(\varphi)} - \frac{1-k_e}{m_e}(T - T_A), \quad (41)$$

and, using the definition (19), the dimensionless diffusion coefficient is

$$\hat{D}(\varphi) = D(\varphi)/D_L = D_S/D_L + p(\varphi)(1 - D_S/D_L). \quad (42)$$

Equations (38) and (39) include the interfacial and bulk characteristic speeds as presented in Table I. Using the analytic expressions from this table, the bulk speeds may have infinite values $V_D^B \to \infty$ and $V_\varphi^B \to \infty$ within the local equilibrium limits $\tau_D \to 0$ and $\tau_\varphi \to 0$. In this case, the system (38) and (39) transforms into the parabolic EFKP model.

## V. NUMERICAL SOLUTION

### A. Method of solution

Taking the first integral from Eq. (38), we arrive at the following equation for solute diffusion:

$$\bar{D}(\varphi)\frac{dC}{dx} + \Theta(\varphi)\hat{D}(\varphi)C\frac{dp(\varphi)}{d\varphi}\frac{d\varphi}{dx} + \frac{V}{V_D^I}(C - C_0) = 0. \quad (43)$$

In this equation, the dimensionless diffusion parameter

$$\bar{D}(\varphi) = \left(\hat{D}(\varphi) - \left(V/V_D^B\right)^2\right)\theta\left[\hat{D}(\varphi) - \left(V/V_D^B\right)^2\right] \quad (44)$$

is introduced with the Heaviside function

$$\theta[r] = \begin{cases} 1, & r > 0, \\ 0, & r \leqslant 0. \end{cases} \quad (45)$$

The definition of parameter (44) takes into account the extremely fast propagation of the interface when $\hat{D}(\varphi) - (V/V_D^B)^2 < 0$. The latter inequality leads to the diffusion field instability and abnormal increase of computed values for concentrations (that can be obtained numerically). This instability follows from the fact that diffusion has no time to act in the rapidly crystallizing local bulk of the system in which the interface velocity $V$ is greater than the diffusion speed $V_D^B$ in bulk liquid. Therefore instead of the difference $\hat{D}(\varphi) - (V/V_D^B)^2$ appearing after the first integration of Eq. (38), we introduce the diffusion parameter (44), which exhibits suppression of the atomic diffusion when $\hat{D}(\varphi) - (V/V_D^B)^2 < 0$.

Equations (43)–(45) are solved numerically by the Runge-Kutta method simultaneously with the phase-field equation (39) resolved by the relaxation method as follows:

$$\frac{\partial\varphi}{\partial\xi_{\rm rel}} = \left[1 - \left(V/V_\varphi^B\right)^2\right]\frac{\partial^2\varphi}{\partial x^2} + \frac{V}{V_\varphi^I}\frac{\partial\varphi}{\partial x} - \frac{9}{2}\frac{dg(\varphi)}{d\varphi} + \frac{1}{2}\frac{\delta}{d_0}\frac{T}{T_A}\Lambda(T,C,\varphi)\frac{dp(\varphi)}{d\varphi}. \quad (46)$$

Here $\xi_{\rm rel}$ is the relaxation parameter allowing us to find the solution for $\varphi$ by Eq. (46) with appropriate accuracy.

The present phase-field model, Sec. II, is formulated in the isothermal approximation. Therefore, for a given temperature, the interface begins to move with zero velocity at the very beginning of the triggered solidification and it will gradually approach a constant velocity of the steady-state stage. Focusing on the steady-state interface motion given by Eqs. (38) and (39) we exclude the initial transient stage of solidification from consideration. Previous studies of the steady-state sharp interfaces under local nonequilibrium conditions [23] show that the "velocity-temperature relationships" functional dependence $V(T)$ of the interface velocity $V$ on the temperature $T$ can be a multivalued function whereas the reverse function $T(V)$ is always single valued. Therefore by looking for the steady-state numerical solution we change from the temperature to the interface velocity as the input parameter and the corresponding temperature of the system is found during the numerical computations by an artificial relaxation in order to match the position of the phase-field profile in the moving frame.

The origin $x_0 = 0$ of the moving reference frame is placed in the point $\varphi = 1/2$ of the diffuse interface, therefore the temperature $T$ is relaxed by

$$\frac{1}{T_A}\frac{\partial T}{\partial\xi_{\rm rel}} = \frac{1}{\xi_V}\frac{\partial x_0}{\partial\xi_{\rm rel}} + \frac{1}{\xi_X}x_0. \quad (47)$$

Here $\xi_V$ and $\xi_X$ are numeric parameters of relaxation which allow us to quickly and self-consistently obtain temperature $T$ and the center $x_0 = 0$ of the diffuse interface. Indeed, the first term on the right hand side of Eq. (47) gives a feedback from the temperature to the relative interface velocity in the moving reference frame to reach $\partial x_0/\partial\xi_{\rm rel} \to 0$. The second term on the right hand side of Eq. (47) "attracts" the moving interface to the point $\varphi = 1/2$ providing $x_0 \to 0$. In limiting cases $\partial\varphi/\partial\xi_{\rm rel} \to 0$ and $\partial T/\partial\xi_{\rm rel} \to 0$, one obtains the stationary profiles of $\varphi(x)$ and $C(x)$ in the moving reference frame. These limits are provided by choosing appropriate values for the parameters $\eta_V$ and $\eta_X$ used for optimizing the relaxation process. For a given interface velocity $V$, the relaxation takes about $10^3 \ldots 10^5$ iterations with the step $d\xi_{\rm rel} \approx 0.01$ depending on the initial approximation and the value of $V$.

The initial condition for $\varphi$ is taken as the diffuse step function (14) at the temperatures below liquidus temperatures.

Boundary conditions for the phase field are $\varphi(\infty) = 1$ and $\varphi(-\infty) = 0$.

Because Eq. (43) is a first-order differential equation, it does not require specific boundary conditions for the concentration field. Therefore we found the solution of Eqs. (43)–(45) for $\bar{D}(\varphi) > 0$ within the Cauchy problem. The special three cases (i) $(V/V_D^B)^2 < D_S/D_L$, (ii) $V/V_D^B > 1$, and (iii) $D_S/D_L \leqslant (V/V_D^B)^2 \leqslant 1$ are specified in the numerical solution as described in Ref. [11].

### B. Definition of the chemical segregation coefficient

The solute trapping effect is evaluated by the chemical segregation coefficient $k(V)$ (which is also known as the solute partitioning function), given by definition (1). To extract the segregation coefficient $k(V)$ from results of the phase-field modeling, several definitions of the $k(V)$ function were given previously.

Ahmad *et al.* [7] defined the $k(V)$ function by the ratio

$$k(V) = \frac{C_S}{C_L} = \frac{C|_{\varphi=0.001}}{\max(C)}. \tag{48}$$

As a result, definition (48) introduces the solute concentration in solid through the concentration at the end of the diffuse interface and the liquid concentration by the concentration maximum.

Danilov and Nestler [9] made an attempt to describe experimental data on solute trapping in the Si-9 at.% As alloy by specific definition of the solute segregation coefficient in the WBM-type parabolic model. They suggested to take the ratio of concentrations at some equidistance $x = \pm\delta_{\text{eff}}$ from the "center" $x = 0$ of the diffuse interface. Ends of this distance, $x = -\delta_{\text{eff}}$ and $x = +\delta_{\text{eff}}$, belong to the solid and liquid phases, respectively, from both sides of the diffuse interface. In this case, the solute segregation coefficient has been defined as

$$k(V) = \frac{C_S}{C_L} = \frac{C|_{x=-\delta_{\text{eff}}}}{C|_{x=+\delta_{\text{eff}}}}, \quad \text{with} \quad \delta_{\text{eff}} = 0.65\delta. \tag{49}$$

Lebedev *et al.* [11] have used a definition for the function $k(V)$ through concentrations at the ends of the diffuse interface as is presented in Fig. 2. Their definition of the $k(V)$ function is given by

$$k(V) = \frac{C_S}{C_L} = \frac{C|_{\varphi=0.001}}{C|_{\varphi=0.999}}. \tag{50}$$

They analyzed the $k(V)$ function predicted by both parabolic and hyperbolic WBM models. It has been found that the complete solute trapping, $C_L = C_S$ and $k(V) = 1$, occurs at a finite crystal growth velocity. However, the complete trapping has begun in that modeling not exactly at a finite velocity which equals the solute diffusion speed $V = V_D^B$, but at smaller values $V < V_D^B$. This result is attributed to the definition (50), which only gives asymptotical values for the ends of the diffuse interface in the nonequilibrium steady-state interfacial motion. With regard to phenomenon of the complete solute trapping, this result would be also expected from definitions (48) and (49).

In the present work we use another definition for the segregation coefficient. *First*, the continuous concentration $C(x)$ is represented through the solute concentration in the liquid, $C_L$, and the solute concentration in the solid, $C_S$. *Second*, the representation is made by a specifically defined function $h(\varphi)$, which provides smooth behavior of $C_L$ and $C_S$ through the interface with the continuous approaching phases. *Third*, the segregation coefficient of the solute is defined by the maxima of liquid and solid concentrations, such that

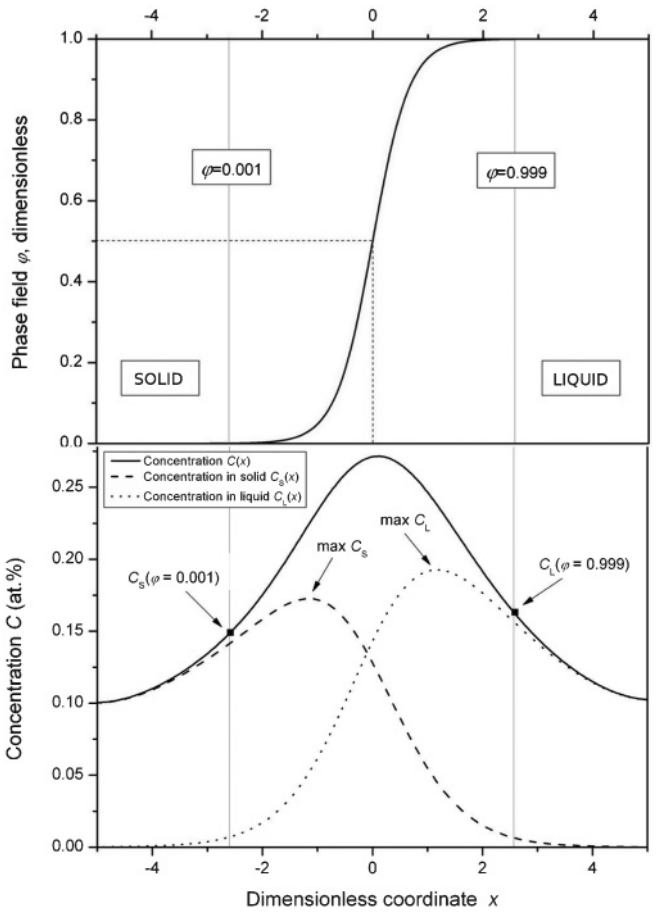


FIG. 2. Concentration profiles used in the definition of the solute segregation coefficient $k(V)$. The upper figure shows phase-field profile with values at the ends of the diffuse interface at which concentrations $C_S$ and $C_L$ in the bottom figure define segregation coefficient (50). In the bottom figure, dashed line presents profile of $C_S$ by Eq. (59) and dotted line presents profile of $C_L$ by Eq. (60). Indicated maxima of these profiles define segregation coefficient by Eq. (51).

$$k(V) = \frac{\max(C_S(x))}{\max(C_L(x))}. \tag{51}$$

These maxima of concentration from definition (51) are shown schematically in Fig. 2.

To define liquid and solid concentrations, we introduce the function $h(p(x))$, which provides monotonic behavior for equilibrium profiles $C_s(x)$ and $C_l(x)$. Therefore consider a solution for concentration profile at equilibrium, i.e., at $V = 0$:

$$C(x) = C_{L\infty}[k_e + (1 - k_e)p(\varphi)], \tag{52}$$

where $C_{L\infty}$ is the solute concentration in bulk liquid. Splitting $C(x)$ on concentration in the liquid, $C_l(x)$, and the solid, $C_s(x)$, gives

$$C(x) = C_s(x) + C_l(x), \tag{53}$$

$$C_s(x) = [1 - h(p(\varphi))]C(x), \tag{54}$$

$$C_l(x) = h(p(\varphi))C(x), \tag{55}$$

where $h(p)$ is a function which must be defined. For the appropriate explicit form of $h(p)$, we add the following condition:

$$C_l(x) = C_{S\infty}p(\varphi) = k_e C_{L\infty}p(\varphi). \tag{56}$$

Using Eqs. (54)–(56), the function $h(p)$ is obtained as

$$h(p) = \frac{p(\varphi)}{k_e + (1 - k_e)p(\varphi)}. \tag{57}$$

As a result, Eq. (57) redefines concentrations $C_l(x)$ and $C_s(x)$ through the function $h(p)$ in such a way that the conditions $h(0) = 0$ and $h(1) = 1$ are satisfied.

Now, introduce the dependence of $h(p)$ on velocity $V$ such that at $V = 0$ one gets $h(p,V) = h(p)$ as is given by Eq. (57). Also, $h(p,V)$ must be a monotonic function of $\varphi$ with the conditions $h[p(\varphi = 0),V] = 0$ and $h[p(\varphi = 1),V] = 1$ at any $V$. Therefore the function $h(p)$ in nonequilibrium can be chosen as [24]

$$h(p,V) = \frac{p(\varphi)}{k(V) + [1 - k(V)]p(\varphi)}, \tag{58}$$

where the solute segregation coefficient is given by Eq. (51). Then, concentrations $C_L(x)$ and $C_S(x)$ are defined by

$$C_S(x) = [1 - h(p,V)]C(x), \tag{59}$$

$$C_L(x) = h(p,V)C(x). \tag{60}$$

With the defined concentrations (59) and (60), the segregation coefficient (51) is used in the present work to evaluate the solute trapping effect. Numerically, this evaluation consists of an iteration process in which a new value $k_{j+1}(V)$ defined

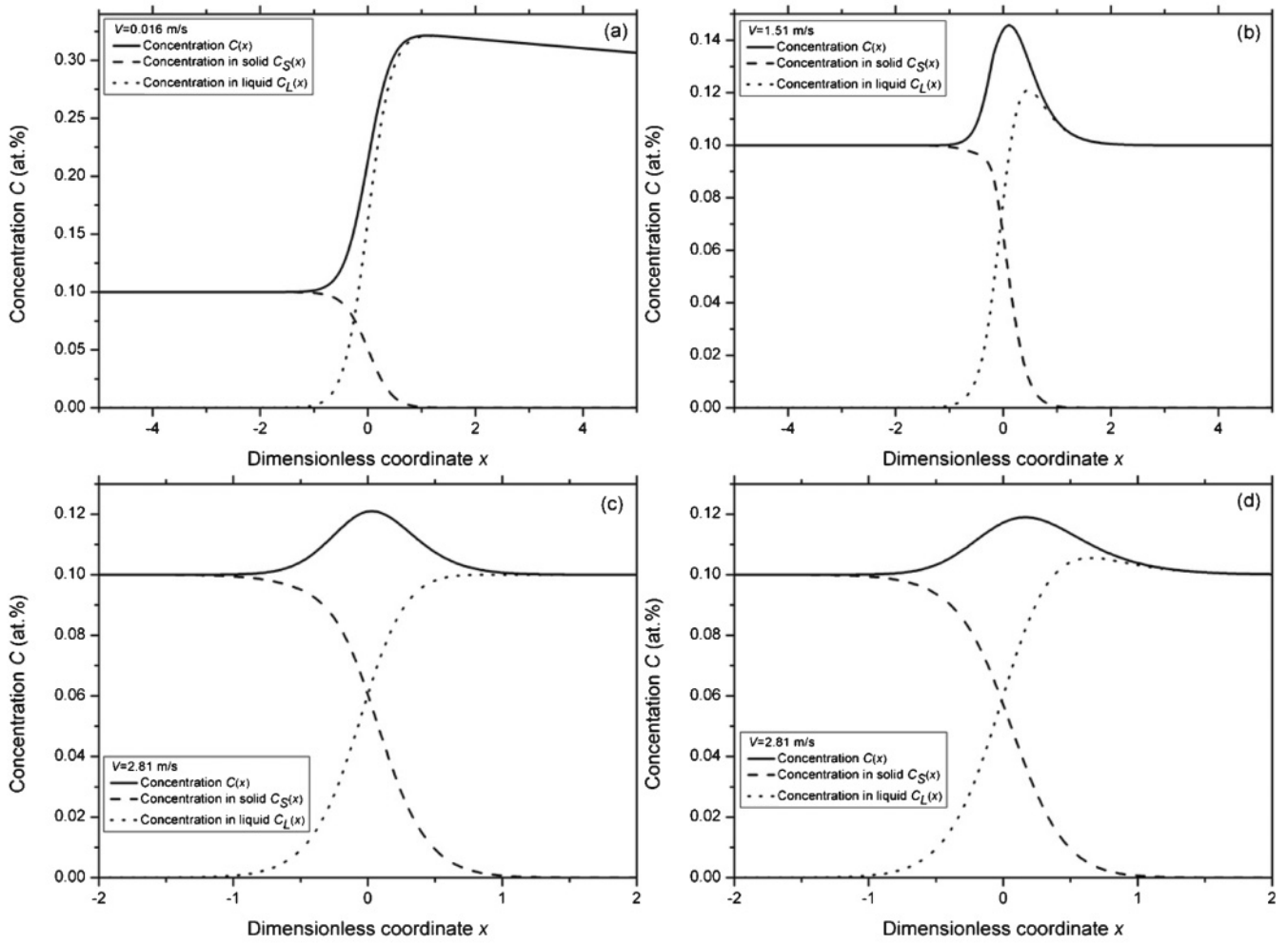


FIG. 3. Concentration profiles for different interface velocities $V$. Continuous lines present $C(x)$ profiles given by solution of Eqs. (43)–(47). Solid concentration $C_S(x)$ and liquid concentration $C_L(x)$ (given by dashed and dotted lines, respectively) are computed using the $C(x)$ profiles by Eqs. (58)–(60). (a) Prediction of the hyperbolic EFKP model at $V = 0.016$ (m/s) $\ll V_D^B$. (b) Prediction of the hyperbolic EFKP model at $V = 1.51$(m/s)$\lesssim V_D^B$. (c) Prediction of the hyperbolic EFKP model at $V = 2.81$ (m/s) $> V_D^B$. (d) Prediction of the parabolic EFKP model [14] at $V = 2.81$ (m/s).

TABLE II. Physical parameters of the Si-0.1 at.% As alloy used for phase-field modeling.

| Parameter | Value | Reference |
|---|---|---|
| $T_A$ | 1685 K | [25] |
| $m_e$ | −400 K/at. frac. | [9] |
| $k_e$ | 0.3 | [26] |
| $v_m$ | $1.2 \times 10^{-5}$ m$^3$/mole | [9] |
| $D_L$ | $1.5 \times 10^{-9}$ m$^2$/s | [26] |
| $D_S$ | $3 \times 10^{-13}$ m$^2$/s | [26] |
| $\sigma$ | 0.477 J/m$^2$ | [25] |
| $\nu$ | $1.57 \times 10^{-8}$ m$^2$/s | present work |
| $\delta$ | $1.875 \times 10^{-9}$ m | [11] |
| $\tau_\varphi$ | $1.0 \times 10^{-11}$ s | [11] |
| $\tau_D$ | $2.4 \times 10^{-10}$ s | from Table I |
| $V_\varphi^I = \nu/\delta$ | 8.37 m/s | from Table I |
| $V_\varphi^B = (\nu/\tau_\varphi)^{1/2}$ | 39.6 m/s | from Table I |
| $V_D^I = D_L/\delta$ | 0.8 m/s | [10] |
| $V_D^B = (D_L/\tau_D)^{1/2}$ | 2.5 m/s | [10] |

by Eq. (51) is obtained by the functions (58)–(60) having the value $k_j(V)$ from the previous $j$th iteration.

## VI. RESULTS OF MODELING

We consider the specific case of a Si-0.1 at.% As alloy with material parameters given in Table II. Numerical solutions for the parabolic EFKP-model [14] are obtained by solving Eqs. (43), (46), and (47) [together with Eqs. (19), (41), and (42)] with the local equilibrium limits $V_D^B \to \infty$ and $V_\varphi^B \to \infty$. The full hyperbolic extension of the EFKP model is given by the governing equations (43) and (46) [using Eqs. (41) and (42), the diffusion parameters (44) and (45), the temperature relaxation expression (47), and the boundary and initial conditions as is given in Sec. V A]. The predictions of the parabolic EFKP model and its hyperbolic extension are compared for the obtained results of concentration fields (Fig. 3), the solute trapping by the solute segregation coefficient on a diffuse interface (Fig. 4), and the kinetic phase diagrams (Figs. 6 and 7).

### A. Concentration profiles

The change in the concentration profile (for atoms of As considered as solute in the Si-0.1 at.% As alloy) with the increase of interface velocity is shown in Fig. 3. It is seen that the width of concentration profile in the liquid in front of the interface of the present hyperbolic extension of the EFKP model shrinks as the velocity increases. Moreover, maximum of the $C(x)$ profile localizes within the diffuse interface and shifts exactly to the center of the interface $x = 0$ as the velocity $V$ increases [see Figs. 3(b) and 3(c)]. This numeric result agrees well with the outcome from analytical treatment given in Sec. III B where localization of the maximum in $C(x)$ is explained by the specific coupling between the concentration and phase fields.

Predictions of the hyperbolic phase-field model give equal maximum values for $C_S(x)$ and $C_L(x)$ at the interface velocity equal to or greater than the solute diffusion speed in bulk liquid, i.e., at $V \geqslant V_D^B$. This result is presented in Fig. 3(c) for the interface velocity $V = 2.81$ (m/s) $> V_D^B$. Contrary to that, the parabolic phase-field model does not converge to this result: $\max(C_S(x)) \neq \max(C_L(x))$ with the finite velocities $V \geqslant V_D^B$ as is shown in Fig. 3(d).

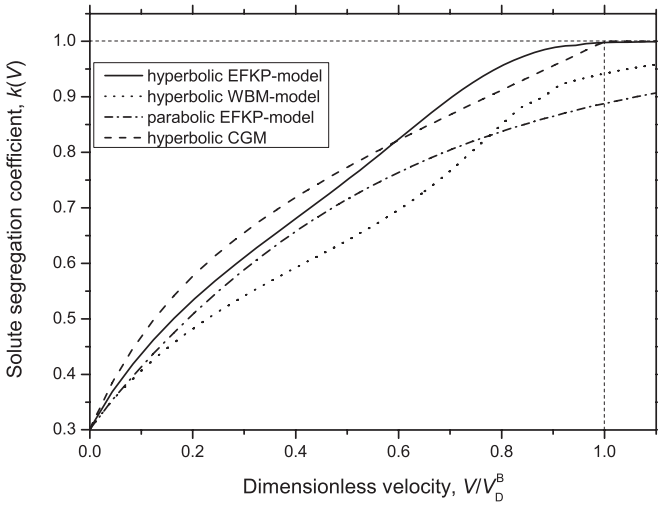


FIG. 4. Nonequilibrium solute segregation coefficient $k(V)$ for Si-0.1 at.% As alloy. Results of the modeling are given for the present hyperbolic EFKP model (solid line) in comparison with the hyperbolic WBM model [11] (dotted line), parabolic EFKP model (dashed-dotted line) [14], and hyperbolic CGM model [10] (dashed line). For EFKP and WBM models the coefficient $k(V)$ was defined by Eqs. (51) and (58)–(60).

### B. Solute segregation

The solute segregation coefficient (1) has been obtained by the definition Eq. (51) in which maximum concentration values are found from Eqs. (58)–(60). These maxima are shown schematically in Fig. 2 and have been obtained from results of modeling shown in Fig. 3. The $k(V)$ function has been evaluated by the results of the present hyperbolic EFKP model, the previously developed hyperbolic WBM model [11], and the kinetic model [10], which can be considered as a hyperbolic extension of the continuous growth model (CGM model). The latter gives analytical expression for the segregation coefficient as

$$k(V, C_{L\infty}) = \frac{\left[1 - V^2/\left(V_D^B\right)^2\right][k_e + (1-k_e)C_{L\infty}] + V/V_D^I}{1 - V^2/\left(V_D^B\right)^2 + V/V_D^I}, \quad V < V_D^B,$$
$$k(V, C_{L\infty}) = 1, \quad V \geqslant V_D^B, \tag{61}$$

where $C_{L\infty}$ is the initial (nominal) concentration having dimension of the atomic fraction. Equation (61) predicts that the transition from chemical partition growth at $V < V_D^B$ to chemical partitionless (diffusionless) growth at $V > V_D^B$ occurs at $V = V_D^B$ abruptly. Such behavior in trapping of solute atoms is also obtained in molecular dynamic simulations [13].

As is shown in Fig. 4, the hyperbolic EFKP model predicts the behavior closely following the analytical expression (61). At $V \geqslant V_D^B$ the complete solute trapping, $k(V) = 1$, is predicted by both these models. This result is

qualitatively consistent with experimental findings and results of molecular dynamic simulations (see results and discussions in Refs. [10,11]). Contrary to this, the hyperbolic WBM model predicts a gradual increase of the nonequilibrium solute segregation coefficient $k(V)$ with absence of the complete solute trapping. Figure 4 demonstrates that this prediction lies below the analytical curve (61) in the entire region of the interface velocity $V$ investigated. We observed, indeed, that $\max(C_S(x)) < \max(C_L(x))$ and $k(V) < 1$ according to definition (51) for all values of $V$ used in simulations by the hyperbolic WBM model. The reason for such behavior is in a difference between chemical driving forces for the WBM and EFKP models. Indeed, the difference of chemical potentials at the temperature $T$ and at the equilibrium temperature $T_A$ is given by, for the WBM model (see Appendix C1 ),

$$\Delta\mu_{\rm WBM} \equiv \mu_{\rm WBM}(T,C,\varphi) - \mu_{\rm WBM}(T_A,C,\varphi) = \frac{RT_A}{v_m}\ln\left(\frac{C^{T/T_A}}{C_l\exp\{[1-p(\varphi)]\Theta T/T_A\}}\right), \quad (62)$$

with $\Theta = \ln k_e$, and for the EFKP model (see Appendix C 2),

$$\Delta\mu_{\rm EFKP} \equiv \mu_{\rm EFKP}(T,C,\varphi) - \mu_{\rm EFKP}(T_A,C,\varphi) = \frac{RT_A}{v_m}\ln\left(\Theta(\varphi)\frac{C^{T/T_A}}{C_l(k_e-1)}\right), \quad (63)$$

where $C_l$ is the equilibrium liquid concentration and $\Theta(\varphi)$ is given by Eq. (40). Thus from concentration profiles $C(x)$, phase-field profiles $\varphi(x)$, and obtained temperature $T$ (i.e., given interface velocity $V$) one can predict the spatial distribution for chemical potentials difference $\Delta\mu(x)$. At equilibrium, both models have zero driving forces for solute diffusion, $\Delta\mu_{\rm WBM} = \Delta\mu_{\rm EFKP} = 0$, as is shown in Fig. 5(a). However, with the increase of velocity $V$, chemical potentials increase in solid in comparison with their equilibrium values as is shown in Figs. 5(b) and 5(c). In this case, the chemical potential difference for the EFKP model is larger than the potentials difference for the WBM model, $|\Delta\mu_{\rm EFKP}| > |\Delta\mu_{\rm WBM}|$, within the diffuse interface. This is presented in Fig. 5(d) for the chemical partition growth with

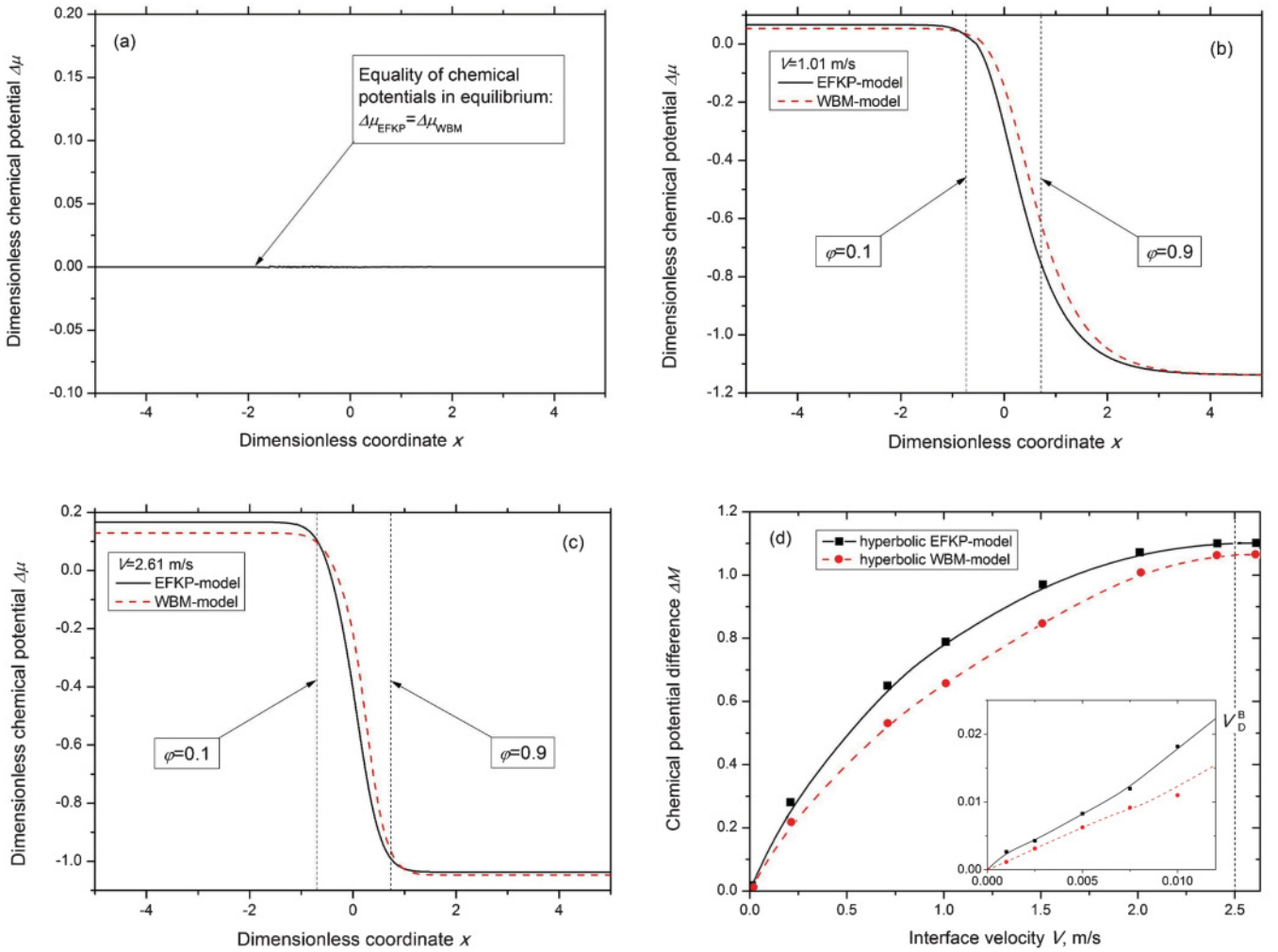


FIG. 5. (Color online) Spatial distribution of chemical potentials for the hyperbolic WBM and EFKP models calculated by Eqs. (62) and (63) and given in the dimensionless form $\Delta\mu_{\rm WBM}/(RT_A/v_m)$ and $\Delta\mu_{\rm EFKP}/(RT_A/v_m)$. (a) Chemical potentials' difference at equilibrium, $V \to 0$. (b) Chemical potentials' difference at $V = 1.01$ (m/s) $\lesssim V_D^B$. (c) Chemical potentials' difference at $V = 2.61$ (m/s) $> V_D^B$. (d) Dimensionless difference $\Delta M(V) = |\Delta\mu(\varphi = 0.9) - \Delta\mu(\varphi = 0.1)|/(RT_A/v_m)$ in chemical potentials for given values of the field variable $\varphi = 0.1$ and $\varphi = 0.9$ [as shown in (b) and (c)]. Inset shows $\Delta M(V)$ function at very small interface velocity, $V \ll V_D^B$.

solute trapping at $V < V_D^B$ and for the diffusionless growth with the complete solute trapping at $V \geqslant V_D^B$. Because the differences $\Delta\mu$ are related to the $\Theta$ functions introduced in the transport equation (38) for both models (see also [11]), the larger values of $\Delta\mu$ provide stronger diffusion redistribution of solutal atoms. Therefore with $\Delta\mu_{\mathrm{EFKP}} > \Delta\mu_{\mathrm{WBM}}$, the driving force in the EFKP model provides solute diffusion in such a way that $\max(C_S(x)) = \max(C_L(x))$ with the complete solute trapping, $k(V) = 1$ at $V \geqslant V_D^B$, and the driving force in the WBM model provides $\max(C_S(x)) < \max(C_L(x))$ with incomplete solute trapping for all investigated $V$ (Fig. 4).

Finally, Fig. 4 clearly shows that the prediction of the present hyperbolic EFKP model and the prediction of the parabolic EFKP model [14] are almost the same for solute partitioning in the range of small and moderate velocity, $0 < V/V_D^B < 0.4$. However, for $V/V_D^B > 0.4$ the hyperbolic EFKP model predicts a steeper behavior for the $k(V)$ function than the parabolic EFKP model. This results in the complete solute trapping predicted by the hyperbolic EFKP model at $V/V_D^B = 1$ and a gradual increasing of the $k(V)$ function with the increase of $V$ by the prediction of the parabolic EFKP model. Such difference in behavior of the nonequilibrium solute partitioning is known from the analysis of the kinetic models based on the continuous growth model [10].

### C. Kinetic phase diagrams

By the definition [27], the kinetic phase diagram presents temperature and chemical composition at the solidification front moving with nonzero velocity $V$ in a steady-state regime. With increasing $V$, kinetic liquidus and solidus lines deviate more pronouncedly from their equilibrium lines and characterize chemical inhomogeneity in the nonequilibrium solid state upon solidification.

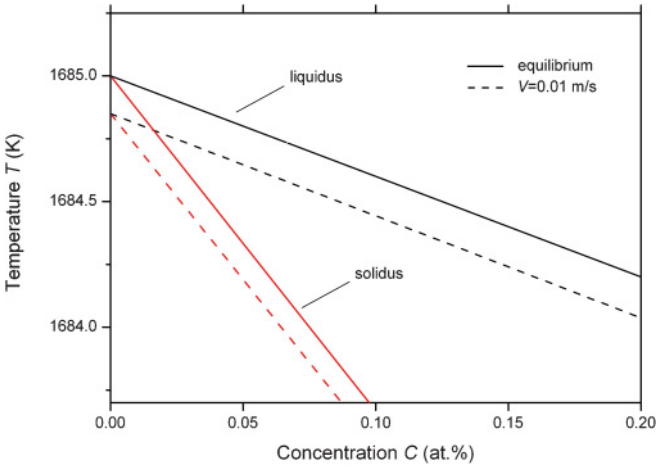


FIG. 6. (Color online) Kinetic phase diagram with the linear approximation of liquidus and solidus lines for Si-As alloys derived from the present hyperbolic EFKP model. Solid lines represent equilibrium lines of the liquidus and solidus. Dashed lines give kinetic liquidus and solidus. Shift of the kinetic liquidus and solidus from their equilibrium positions is shown at the interface velocity $V = 0.01$ (m/s) $\ll V_D^B$.

It is straightforward to show that, using a common tangent construction, the accepted dilute alloy approximation leads to straight lines of the solidus $T_S = T_A + m_e C_s$ and the liquidus $T_L = T_A + m_e C_l$ in the phase diagram with the tangent $m_e = -(1 - k_e)(RT/v_m)(T_A/L)$ of the liquidus line and with the relation between equilibrium concentrations as $C_s = k_e C_l$ (see Appendix A 1). Kinetic phase diagrams can be drawn relative to these equilibrium lines $T_S(C_s)$ and $T_L(C_l)$.

Figures 6 and 7 exhibit kinetic phase diagrams of alloy rapid solidification in the coordinates "interface temperature and concentration" constructed using modeling results of the hyperbolic extension of the EFKP model. The interval of solidification, as a distance between lines of liquidus and solidus, shrinks with the increase of interface velocity $V$. This is clearly seen by comparing the solid lines for the equilibrium state with $V = 0$ (m/s) and the dashed lines for kinetic liquidus and solidus lines for $V = 0.01$ (m/s), shown in Fig. 6. With a higher interface velocity, $V \geqslant V_D^B$, the kinetic liquidus and solidus lines merge into one line, shown as a dashed line in Fig. 7. This result indicates the equality of solid and liquid concentrations on both sides of the diffuse interface: in the modeling we obtained

$$\max(C_S(x)) = \max(C_L(x)) \equiv C_{L\infty} \quad \text{with} \quad k(V) \equiv 1.$$

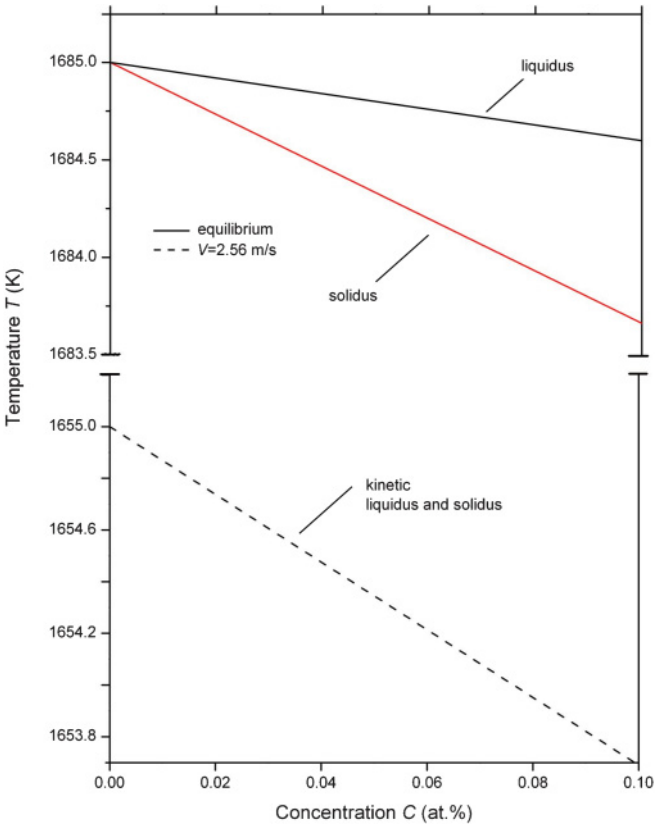


FIG. 7. (Color online) Kinetic phase diagram with the linear approximation of liquidus and solidus lines for Si-As alloys derived from the present hyperbolic EFKP model. Solid lines represent equilibrium lines of the liquidus and solidus. Confluence of the kinetic liquidus and solidus in a single dashed line is shown as a result of the complete solute trapping and diffusionless solidification at the interface velocity $V = 2.56$ (m/s) $> V_D^B$.

This result can be recognized as one of the main characteristics of complete solute trapping that accompanies diffusionless solidification.

Note that using the parabolic system of phase-field equations one can find that kinetic liquidus and solidus lines only gradually approach each other as the velocity $V$ increases (see, e.g., the kinetic diagram in Fig. 4 of Ref. [8]). Chemically partitionless solidification is also predicted previously using a sharp-interface model in which solute transport has been described by the hyperbolic equation (see, e.g., the kinetic diagram in Fig. 4 of Ref. [28]).

Finally, two features of the kinetic phase diagrams, presented in Figs. 6 and 7, should be outlined. First, in the present dilute alloy approximation, we have straight lines for the kinetic liquidus and solidus. This follows from Taylor expansions of the liquidus and solidus temperatures,

$$T_L(V,C) = T_A + m(V)C + \mathcal{O}(C^2),$$
$$T_S(V,C) = T_A + m(V)C/k(V) + \mathcal{O}(C^2),$$

which show that by dropping high-order terms $\mathcal{O}(C^2)$ in the dilute limit we get straight lines for the liquidus and solidus for the equilibrium and nonequilibrium states. Of course, the liquidus slope $m(V)$ as well as the partition coefficient $k(V)$ remain velocity dependent functions and vary between equilibrium and nonequilibrium. *Second*, for the pure one-component system, the change of the temperature $T$ with respect to equilibrium solidification temperature $T_A$ is described by [see Eqs. (B24)–(B27)]

$$T(V,C=0) = T_A - \frac{V}{\mu\sqrt{1 - V^2/\left(V_\varphi^B\right)^2}}, \quad \text{with}$$
$$\mu = \frac{\nu L}{\sigma T_A} \quad \text{and} \quad V < V_\varphi^B. \tag{64}$$

From this it follows that the temperature $T(V,C=0)$ deviates from its equilibrium value $T_A$ by the nonlinear law only for the highest velocity $V \approx V_\varphi^B$.

## VII. CONCLUSIONS

The parabolic phase-field model of Echebarria, Folch, Karma, and Plapp (EFKP model) [14] has been extended to the case of local nonequilibrium solidification. Four kinetic parameters appear in the model as main characteristics of local nonequilibrium effects. These are the characteristic speeds of atomic diffusion and phase-field propagation within and around the moving diffuse solid-liquid interface (see Table I). The resulting model is described by a system of hyperbolic partial differential equations for the atomic diffusion transport and diffuse interface advancement.

The present hyperbolic EFKP model is applied to the solute trapping problem. Modeling results have been analyzed by considering solute concentration profiles, the solute segregation coefficient, and kinetic phase diagrams.

Predictions of the parabolic EFKP model [14] have been compared with the results of the presently developed hyperbolic EFKP model. As it is shown, the hyperbolic model predicts the complete solute trapping beginning at the fixed interface velocity equal to the maximum diffusion speed $V = V_D^B$. At this critical point, the alloy solidifies as a supersaturated solid solution with the initial (nominal) chemical composition. With the velocity $V > V_D^B$, solidification proceeds by the diffusionless mechanism whose rate is bounded above by the maximum speed for phase-field propagation, i.e., $V < V_\varphi^B$. Indeed, for the hyperbolic equation of the phase field, we have found step solutions (B18), (B22), and (B24) in regimes $V < V_\varphi^B$. Possible solutions for $V \geqslant V_\varphi^B$ might be obtained together with their stability analysis, existence, and uniqueness. Finally, to compare modeling predictions with experimental data, the model can be generalized to nonideal solutions and concentrated binary systems.

## ACKNOWLEDGMENTS

We thank Mathis Plapp, Ingo Steinbach, Dmitry Medvedev, and Oleg Shchyglo for numerous fruitful discussions and useful suggestions. P.K.G. and D.M.H. acknowledge support from DFG (German Research Foundation) under Project No. HE 160/19 and DLR Space Management under Contract No. 50WM1140. E.V.A. acknowledges support from DAAD (German Academic Exchanges Service) under Stipendium A/08/81583. D.J. acknowledges support by the Direccion General de Investigación of the Spanish Ministry of Education and Science under Grant No. Fis 2009-13370-C02-01 and of the Generalitat of Catalonia under Grant No. 2009-SGR-00164. D.A.D. acknowledges support from RFBR (Russian Foundation of Basic Research) under Project No. 09-02-12110-ofi-m. V.G.L. acknowledges support from RFBR (Russian Foundation of Basic Research) under Project No. 08-02-91957NNIO_a and from ROSNAUKA (Russian Scientific Foundation) under Project No. 2009-1.5-507-007-002.

## APPENDIX A: EQUILIBRIUM FEATURES AND PROFILES OF THE PHASE FIELD

Equilibrium conditions in the phase-field model are given by

$$\frac{\delta F}{\delta \varphi} = 0, \quad \frac{\delta F}{\delta C} = \mu_{\rm eq}(T), \tag{A1}$$

where $\mu_{\rm eq}(T) = \mu(\varphi,C,T)$. The measure of equilibrium, the chemical potential $\mu_{\rm eq}$, can be obtained from equilibrium free energy densities in both phases, $f_s(C,T)$ and $f_l(C,T)$, by

$$\left.\frac{\partial f_s(C,T)}{\partial C}\right|_{C=C_s} = \left.\frac{\partial f_l(C,T)}{\partial C}\right|_{C=C_l} = \mu_{\rm eq}(T), \tag{A2}$$

$$f_s(C_s,T) - \mu_{\rm eq}C_s = f_l(C_l,T) - \mu_{\rm eq}C_l, \tag{A3}$$

where $C_s$ and $C_l$ are equilibrium concentrations in solid and liquid, respectively. Equations (A2) and (A3) are used in this section to obtain equilibrium concentration and phase-field profiles as described by EFKP and WBM models [5,14].

### 1. Equilibrium features of the EFKP model

In the free energy density (4) the entropy density $s(\varphi)$ and inner energy $\epsilon(\varphi)$ include interpolation functions $p_s(\varphi)$ and

$p_\epsilon(\varphi)$ and are given by [14]

$$s(\varphi) = \frac{s_s + s_l}{2} - p_s(\varphi)\frac{L}{2T_A}, \tag{A4}$$

$$\epsilon(\varphi) = \frac{\epsilon_s + \epsilon_l}{2} + p_\epsilon(\varphi)\frac{\Delta\epsilon}{2}, \tag{A5}$$

where $\Delta\epsilon = \epsilon_s - \epsilon_l$, $L = T_A(s_l - s_s)$. The functions $p_s$ and $p_\epsilon$ satisfy the following conditions:

$$\begin{aligned} &p_s(0) = p_\epsilon(0) = 1, \quad p_s(1) = p_\epsilon(1) = -1, \\ &\left.\frac{dp_s(\varphi)}{d\varphi}\right|_{\varphi=0} = \left.\frac{dp_\epsilon(\varphi)}{d\varphi}\right|_{\varphi=0} = 0, \\ &\left.\frac{dp_s(\varphi)}{d\varphi}\right|_{\varphi=1} = \left.\frac{dp_\epsilon(\varphi)}{d\varphi}\right|_{\varphi=1} = 0, \end{aligned} \tag{A6}$$

such that the free energy density (4) gives the free energies for the liquid and solid phases as follows:

$$\begin{aligned} f_s(C_s,T) = {} & f^A(T_A) - (T - T_A)s_s \\ & + \epsilon_s C_s + \frac{RT_A}{v_m}(C_s \ln C_s - C_s), \end{aligned} \tag{A7}$$

$$\begin{aligned} f_l(C_l,T) = {} & f^A(T_A) - (T - T_A)s_l \\ & + \epsilon_l C_l + \frac{RT_A}{v_m}(C_l \ln C_l - C_l). \end{aligned} \tag{A8}$$

Choosing $p_s$ by Eq. (6), from Eqs. (A7) and (A8) follows

$$\frac{\partial f_s}{\partial C_s} = \epsilon_s + \frac{RT_A}{v_m}\ln C_s, \tag{A9}$$

$$\frac{\partial f_l}{\partial C_l} = \epsilon_l + \frac{RT_A}{v_m}\ln C_l. \tag{A10}$$

Substituting Eqs. (A9) and (A10) into definition (A3) gives the equilibrium chemical potential

$$\epsilon_s + \frac{RT_A}{v_m}\ln C_s = \epsilon_l + \frac{RT_A}{v_m}\ln C_l = \mu_{\rm eq}, \tag{A11}$$

using of which one can define equilibrium solute partitioning by the solute segregation coefficient:

$$k_e = \frac{C_s}{C_l} = \exp\left(-\frac{v_m}{RT_A}\Delta\epsilon\right). \tag{A12}$$

Further substituting Eqs. (A7) and (A8) into the same definition (A3) with use Eq. (A11) leads to the relation

$$\frac{v_m}{RT}(T - T_A)\frac{L}{T_A} + \frac{v_m}{RT}\Delta\epsilon C_s + C_s \ln k_e - (C_s - C_l) = 0. \tag{A13}$$

With using Eq. (A12), finally, we obtain from Eq. (A13) equilibrium concentrations in phases

$$C_l = \frac{v_m}{RT}\frac{L}{T_A}\frac{1}{1 - k_e}(T_A - T), \quad C_s = k_e C_l, \tag{A14}$$

and a slope of the liquidus line in equilibrium phase diagram

$$m_e = -(1 - k_e)\frac{RT}{v_m}\frac{T_A}{L}. \tag{A15}$$

**2. Concentration profile and phase-field profile in EFKP model**

Equilibrium profile of concentration for a given value of $\varphi(x)$ is obtained from Eq. (2) by

$$\left(\frac{\partial^2 f}{\partial C^2}\right)\frac{dC}{dx} + \left(\frac{\partial^2 f}{\partial C\,\partial\varphi}\right)\frac{d\varphi}{dx} = \text{const}. \tag{A16}$$

Using expressions for the free energy (4) and internal energy (7), one gets

$$\begin{aligned} &\frac{\partial^2 f}{\partial C^2} = \frac{RT}{v_m C}, \\ &\frac{\partial^2 f}{\partial C\,\partial\varphi} = \frac{d\epsilon(\varphi)}{d\varphi} = -\frac{1}{2}\frac{RT}{v_m}\ln k_e \frac{dp_\epsilon}{d\varphi}. \end{aligned} \tag{A17}$$

Substituting Eq. (A17) into Eq. (A16) leads to

$$\ln C - \frac{p_\epsilon}{2}\ln k_e = \text{const} \equiv 0. \tag{A18}$$

As a result, taking Eq. (A6) into account, the equilibrium concentration profile in the EFKP model is described by

$$C(x) = C_l \exp\left(\frac{\ln k_e}{2}[1 + p_\epsilon(\varphi)]\right). \tag{A19}$$

Phase-field equilibrium follows from Eq. (3) and is given by

$$\begin{aligned} &\varepsilon_\varphi^2\frac{d^2\varphi}{dx^2} - W\frac{dg(\varphi)}{d\varphi} \\ &\quad = \frac{1}{2}\frac{dp_s(\varphi)}{d\varphi}\frac{T - T_A}{T_A}L + \frac{1}{2}\frac{dp_\epsilon(\varphi)}{d\varphi}\Delta\epsilon C_0. \end{aligned} \tag{A20}$$

Using Eqs. (A12) and (A14) one gets from Eq. (A20) the following equation:

$$\begin{aligned} &\varepsilon_\varphi^2\frac{d^2\varphi}{dx^2} - W\frac{dg(\varphi)}{d\varphi} \\ &\quad = -\frac{RT}{2v_m}C_l\left[(1 - k_e)\frac{dp_s(\varphi)}{d\varphi} + \ln k_e\frac{C(x)}{C_l}\frac{dp_\epsilon(\varphi)}{d\varphi}\right]. \end{aligned} \tag{A21}$$

With the equilibrium condition $\partial f(\varphi,C,T)/\partial\varphi = 0$ and Eq. (A19), one obtains

$$(1-k_e)\frac{dp_s(\varphi)}{d\varphi} + \ln(k_e)\frac{dp_\epsilon(\varphi)}{d\varphi}\exp\left(\frac{\ln k_e}{2}[1+p_\epsilon(\varphi)]\right) = 0. \tag{A22}$$

This condition leads to the definition of functions (6) and (7) and gives zero for the right hand side of Eq. (A21). Then, the equation $\varepsilon_\varphi^2 d^2\varphi/dx^2 - W dg(\varphi)/d\varphi = 0$ has the kink solution:

$$\varphi(x) = \frac{1}{2} + \frac{1}{2}\tanh\left(\frac{3x}{2\delta}\right). \tag{A23}$$

This distribution agrees with the equilibrium $\varphi$ profile (14) in which $\delta = 3\varepsilon_\varphi/\sqrt{2W}$ according to the chosen parameters (36).

### 3. Concentration profile and phase-field profile in WBM model

The free energy density in the Wheeler-Boettinger-McFadden model (WBM model) is given by [5]

$$f_e(C,T,\varphi) = f_A(T,\varphi) + Cf_B(T,\varphi) + \frac{RT_A}{v_m}(C\ln C - C) + Wg(\varphi), \quad \text{(A24)}$$

where the free energies $f_A(T,\varphi)$ and $f_B(T,\varphi)$ of $A$ and $B$ particles are

$$f_A(T,\varphi) = -\frac{RT_A}{v_m}\frac{1-k_e}{m_e}(T-T_A)[1-p(\varphi)], \quad \text{(A25)}$$

$$f_B(T,\varphi) = -\frac{RT_A}{v_m}\ln k_e[1-p(\varphi)]. \quad \text{(A26)}$$

From solution of equilibrium conditions (A2) and (A3) we obtain the equilibrium concentration profile. The free energy densities in phases are

$$f_s(C_s,T) = \frac{RT_A}{v_m}\frac{1-k_e}{m_e}(T_A-T) - C_s\frac{RT_A}{v_m}\ln k_e + \frac{RT_A}{v_m}(C_s\ln C_s - C_s), \quad \text{(A27)}$$

$$f_l(C_l,T) = \frac{RT_A}{v_m}(C_l\ln C_l - C_l). \quad \text{(A28)}$$

Using Eq. (A2), one can obtain from Eqs. (A27) and (A28) the following expressions for equilibrium chemical potentials in phases:

$$\mu_{\rm eq} = \frac{RT_A}{v_m}\ln C_l, \quad \mu_{\rm eq} = -\frac{RT_A}{v_m}\ln k_e + \frac{RT_A}{v_m}\ln C_s. \quad \text{(A29)}$$

Then, from Eq. (A3) the equilibrium concentrations are given by

$$C_l = -\frac{T_A - T}{m_e}, \quad C_s = k_e C_l, \quad \text{(A30)}$$

and the equilibrium concentration profile is

$$C(x) = C_l\exp\{\ln k_e[1-p(\varphi)]\}. \quad \text{(A31)}$$

Note that the above concentrations $C_l$ and $C_s$ as well as the slope $m_e$ completely agree with those ones obtained for the EFKP model, Eqs. (A14) and (A15).

The equilibrium phase-field profile $\varphi(x)$ in Eq. (A31) is defined by

$$\varepsilon_\varphi^2\frac{\partial^2\varphi}{\partial x^2} - \frac{\partial f}{\partial\varphi} = 0. \quad \text{(A32)}$$

Then, taking definitions (A24)–(A26) into account, we obtain

$$\frac{\partial^2\varphi}{\partial x^2} - \frac{9}{2}\frac{dg(\varphi)}{d\varphi} - \frac{1}{2}\frac{\delta}{d_0}\frac{T}{T_A}\left(\frac{1-k_e}{m_e}(T-T_A) + C\ln k_e\right)\frac{dp(\varphi)}{d\varphi} = 0. \quad \text{(A33)}$$

Using Eqs. (A30) and (A31) in Eq. (A33), one gets

$$\frac{\partial^2\varphi}{\partial x^2} - \frac{9}{2}\frac{dg(\varphi)}{d\varphi} = \frac{1}{2}\frac{\delta}{d_0}\frac{T}{T_A}C_l[1-k_e+\ln(k_e)e^{\ln k_e(1-p(\varphi))}]\frac{dp(\varphi)}{d\varphi}. \quad \text{(A34)}$$

This equation gives the phase-field profile with equilibrium coexistence of liquid and crystal in the WBM model.

## APPENDIX B: EQUATIONS OF THE HYPERBOLIC EFKP MODEL

Consider a flat interface between solid and liquid phases moving in perpendicular direction to the $x$ axis. Then one can consider Eqs. (2) and (3) in one spatial dimension.

### 1. Concentration field

To obtain explicit form of one-dimensional equation (2) we use the free energy density, Eqs. (4)–(8), and the derivatives from it, Eq. (A17), such that the mobility is

$$M_C(T,C,\varphi) = \left(\frac{\partial^2 f}{\partial C^2}\right)^{-1} D(\varphi) = \frac{v_m C}{RT}D(\varphi). \quad \text{(B1)}$$

Then, using

$$\frac{dp_\epsilon(\varphi)}{d\varphi} = -\frac{1-k_e}{\ln k_e}\frac{1}{k_e^{(1+p_\epsilon)/2}}\frac{dp_s(\varphi)}{d\varphi} \quad \text{(B2)}$$

with $dp_s/d\varphi = -2dp/d\varphi$ and equality

$$\frac{1}{k_e^{(1+p_\epsilon)/2}} = \frac{1}{k_e+(1-k_e)p(\varphi)}, \quad \text{(B3)}$$

we obtain

$$\frac{\partial^2 f}{\partial C\partial\varphi} = -\frac{RT}{v_m}\frac{1-k_e}{k_e+(1-k_e)p(\varphi)}\frac{dp}{d\varphi}, \quad \text{(B4)}$$

$$M_C\frac{\partial^2 f}{\partial C\partial\varphi} = -D(\varphi)C\frac{1-k_e}{k_e+(1-k_e)p(\varphi)}\frac{dp(\varphi)}{d\varphi}. \quad \text{(B5)}$$

Substituting Eqs. (B1) and (B5) into Eq. (2) gives

$$\tau_D\frac{\partial^2 C}{\partial t^2} + \frac{\partial C}{\partial t} = \frac{\partial}{\partial x}\left(D(\varphi)\frac{\partial C}{\partial x}\right) - \frac{\partial}{\partial x}\left[D(\varphi)C\frac{1-k_e}{k_e+(1-k_e)p(\varphi)}\frac{dp(\varphi)}{d\varphi}\frac{\partial\varphi}{\partial x}\right]. \quad \text{(B6)}$$

Introducing the function

$$\Theta(\varphi) = -\frac{1-k_e}{k_e+(1-k_e)p(\varphi)}, \quad \text{(B7)}$$

one-dimensional Eq. (2) reads in the moving reference frame as

$$\tau_D \frac{v^2}{D_L \delta^2}\frac{\partial^2 C}{\partial t^2} - 2\tau_D \frac{vV}{D_L}\frac{\partial^2 C}{\partial t \partial x} + \frac{\tau_D V^2}{D_L}\frac{\partial^2 C}{\partial x^2} + \frac{v}{D_L}\frac{\partial C}{\partial t} - \frac{V\delta}{D_L}\frac{\partial C}{\partial x} = \frac{\partial}{\partial x}\left(\frac{D(\varphi)}{D_L}\frac{\partial C}{\partial x}\right) + \frac{\partial}{\partial x}\left(\frac{D(\varphi)}{D_L} C\Theta(\varphi)\frac{dp(\varphi)}{d\varphi}\frac{\partial \varphi}{\partial x}\right). \quad \text{(B8)}$$

In a reference frame moving with constant velocity $V$, Eq. (B8) takes the following form:

$$\frac{V^2}{\left(V_D^B\right)^2}\frac{d^2 C}{dx^2} - \frac{V}{V_D^I}\frac{dC}{dx} = \frac{d}{dx}\left(\frac{D(\varphi)}{D_L}\frac{dC}{dx}\right) + \frac{d}{dx}\left(\frac{D(\varphi)}{D_L} C\Theta(\varphi)\frac{dp(\varphi)}{d\varphi}\frac{d\varphi}{dx}\right). \quad \text{(B9)}$$

Equation (B9) has two characteristic diffusion speeds as is given in Table I.

### 2. Phase field

To obtain the explicit form of one-dimensional Eq. (3), which describes evolution of the phase field $\varphi$, we obtain from Eqs. (4)–(8) that

$$\frac{\partial f}{\partial \varphi} = \frac{9\sigma}{\delta}\frac{dg(\varphi)}{d\varphi} - \frac{1}{2}\frac{RT}{v_m}\left(\frac{1-k_e}{m_e}(T - T_A)\frac{dp_s(\varphi)}{d\varphi} + C\ln k_e \frac{dp_\epsilon(\varphi)}{d\varphi}\right). \quad \text{(B10)}$$

Then, using Eqs. (B2) and (B10), one-dimensional Eq. (3) is written as

$$\tau_\varphi \frac{\partial^2 \varphi}{\partial t^2} + \frac{\partial \varphi}{\partial t} = v\frac{\partial^2 \varphi}{\partial x^2} - \frac{9v}{2\delta^2}\frac{dg(\varphi)}{d\varphi} - \frac{vRT}{2\sigma\delta v_m}\left(\frac{1-k_e}{m_e}(T - T_A) - C\frac{1-k_e}{k_e + (1-k_e)p(\varphi)}\right)\frac{dp(\varphi)}{d\varphi}. \quad \text{(B11)}$$

In a moving reference frame Eq. (B11) reads

$$\begin{aligned}&\frac{\tau_\varphi v}{\delta^2}\frac{\partial^2 \varphi}{\partial t^2} - 2\tau_\varphi V\frac{d^2\varphi}{\partial t \partial x} + \frac{\tau_\varphi V^2}{v}\frac{\partial^2 \varphi}{\partial x^2} + \frac{\partial \varphi}{\partial t} - \frac{V\delta}{v}\frac{\partial \varphi}{\partial x}\\ &\quad = \frac{\partial^2 \varphi}{\partial x^2} - \frac{9}{2}\frac{dg(\varphi)}{d\varphi} - \frac{1}{2}\frac{\delta}{d_0}\frac{T}{T_A}\left(\frac{1-k_e}{m_e}(T - T_A) - C\frac{1-k_e}{k_e + (1-k_e)p(\varphi)}\right)\frac{dp(\varphi)}{d\varphi}, \end{aligned} \quad \text{(B12)}$$

where dimensionless time and spatial coordinate were used as described in Sec. IV B. In the case of moving reference frame with constant velocity $V$, Eq. (B12) has the following form:

$$\frac{V^2}{\left(V_\varphi^B\right)^2}\frac{d^2\varphi}{dx^2} - \frac{V}{V_\varphi^I}\frac{d\varphi}{dx} = \frac{d^2\varphi}{dx^2} - \frac{9}{2}\frac{dg(\varphi)}{d\varphi} + \frac{1}{2}\frac{\delta}{d_0}\frac{T}{T_A}\Lambda(T,C,\varphi)\frac{dp(\varphi)}{d\varphi}, \quad \text{(B13)}$$

where we used the function

$$\Lambda(T,C,\varphi) = \frac{(1-k_e)C}{k_e + (1-k_e)p(\varphi)} - \frac{1-k_e}{m_e}(T - T_A). \quad \text{(B14)}$$

Equation (B13) introduces two characteristic speeds for the phase field as is given in Table I.

We specially have to note that transport equation (B9) and equation of motion (B13) are the same as is described by the hyperbolic WBM model. The main difference in the models is that the functions $\Theta(\varphi)$ and $\Lambda(T,C,\varphi)$, which are given by Eqs. (B7) and (B14), respectively, differ substantially from those obtained for the hyperbolic WBM model [11].

In the specific case of a pure material one can obtain from Eq. (B13) an explicit relationship between the interface velocity $V$ and the temperature $T$ or the undercooling $\Delta T = T_A - T$. By setting $C = 0$ for pure substance of $A$ atoms and by taking into account Eq. (A15), the function $\Lambda$ reduces to

$$\Lambda(T) = \frac{v_m L}{RT}\frac{T - T_A}{T_A} = -\frac{v_m L}{RT}\frac{\Delta T}{T_A}. \quad \text{(B15)}$$

For the double-well function $g(\varphi)$ in Eq. (5) and for the interpolation function $p(\varphi)$ in Eq. (8) we have

$$\frac{dg(\varphi)}{d\varphi} = 2\varphi(1-\varphi)(1-2\varphi) \quad \text{(B16)}$$

and

$$\frac{dp(\varphi)}{d\varphi} = 6\varphi(1-\varphi). \quad \text{(B17)}$$

For a steplike phase-field profile

$$\varphi(x) = \frac{1}{2}\left(1 + \tanh\frac{x}{l}\right) \quad \text{(B18)}$$

the derivatives in Eq. (B13) can be expressed as

$$\frac{d\varphi}{dx} = \frac{2}{l}\varphi(1-\varphi) \quad \text{(B19)}$$

and

$$\frac{d^2\varphi}{dx^2} = \frac{4}{l^2}\varphi(1-\varphi)(1-2\varphi). \quad \text{(B20)}$$

The right hand sides in Eqs. (B16) and (B17) and in Eqs. (B19) and (B20) are similar. Therefore substituting these derivatives into Eq. (B13) gives

$$\left[\left(1-\frac{V^2}{\left(V_\varphi^B\right)^2}\right)\frac{4}{l^2}-9\right]\varphi(1-\varphi)(1-2\varphi) + \left[\frac{V}{V_\varphi^I}\frac{2}{l}+3\frac{\delta}{d_0}\frac{T}{T_A}\Lambda(T)\right]\varphi(1-\varphi)=0. \quad \text{(B21)}$$

The first summand gives the expression for the interface thickness $l$ in Eq. (B18),

$$l=\frac{2}{3}\sqrt{1-\frac{V^2}{\left(V_\varphi^B\right)^2}}. \quad \text{(B22)}$$

Note that in the parabolic case with $V_\varphi^B\to\infty$, the interface thickness $l$ has a constant value and the phase-field profile in Eq. (B18) is equal to the equilibrium phase-field profile in Eq. (A23). Taking the relaxation effects into account, it is seen from Eq. (B22) that the interface thickness $l$ gradually decreases toward zero as the interface velocity $V$ increases up to the maximum speed $V_\varphi^B$ for the phase-field propagation.

The second summand in Eq. (B21) gives the relationship between the interface velocity $V$ and the temperature $T$. Indeed, using the expression $V_\varphi^I=\nu/\delta$ from Table I, one gets

$$\frac{V}{\sqrt{1-V^2/\left(V_\varphi^B\right)^2}}=-\frac{\nu}{d_0}\frac{T}{T_A}\Lambda(T). \quad \text{(B23)}$$

Here, the function $\Lambda(T)$ represents the driving force for the phase-field propagation. Taking Eq. (B15) into account, the relationship in Eq. (B23) in terms of the undercooling $\Delta T$ reads

$$\frac{V}{\sqrt{1-V^2/(V_\varphi^B)^2}}=\frac{\nu}{d_0}\frac{v_m L}{RT_A}\frac{\Delta T}{T_A}. \quad \text{(B24)}$$

With the interface velocity much smaller than the maximum speed for the phase-field propagation, $V\ll V_\varphi^B$, one obtains the linear relation

$$V=\mu\Delta T, \quad \text{(B25)}$$

where the kinetic coefficient is given by

$$\mu=\frac{\nu}{d_0}\frac{v_m L}{RT_A^2}. \quad \text{(B26)}$$

Using Eq. (36), the kinetic coefficient related to the surface energy is obtained as

$$\mu=\frac{\nu}{\sigma}\frac{L}{T_A}. \quad \text{(B27)}$$

In summary, we have found solutions for the interfacial thickness (B22) and velocity (B24), which are true for the step form of the phase-field profile (B18) and for the regime $V<V_\varphi^B$. Special consideration of possible solutions for regimes $V\geqslant V_\varphi^B$ might also be presented together with their stability analysis, existence, and uniqueness.

## APPENDIX C: DRIVING FORCES FOR SOLUTE DIFFUSION

### 1. Chemical potential difference for the WBM model

Using the definition $\mu=\partial f/\partial C$ and the free energy (A24)–(A26) one can obtain the chemical potential

$$\mu_{\rm WBM}=-\frac{RT}{v_m}\ln k_e[1-p(\varphi)]+\frac{RT}{v_m}\ln C \quad \text{(C1)}$$

for the phase-field WBM model [5]. Expression (C1) and the equilibrium potential in liquid (A29) give the following difference:

$$\begin{aligned}\Delta\mu_{\rm WBM}&\equiv\mu_{\rm WBM}(T,C,\varphi)-\mu_{\rm WBM}(T_A,C,\varphi)\\&=\frac{RT_A}{v_m}\left[\frac{T}{T_A}\ln C-\frac{T}{T_A}[1-p(\varphi)]\ln k_e-\ln C_l\right]\\&=\frac{RT_A}{v_m}\ln\frac{C^{T/T_A}}{C_l k_e^{[1-p(\varphi)]T/T_A}}.\end{aligned} \quad \text{(C2)}$$

For the equilibrium potential $\mu_{\rm WBM}(T_A,C,\varphi)$ we assume that the equilibrium liquid concentration is $C=C_l$ with $\varphi=1$.

As we noted in the previous section, the solute diffusion equation (B9) is the same for WBM and EFKP models, however, the $\Theta$ function is different for both models. In particular, in the hyperbolic WBM model one finds [11]

$$\Theta=\ln\left(\frac{1+(T_A-T)/m_e}{1+k_e(T_A-T)/m_e}\right)+\ln k_e.$$

At a tiny amount of a solute, the dilute alloy approximation reads $T\to T_A$ and $m_e\to\infty$. Then, the above expression gives $\Theta=\ln k_e$ and Eq. (C2) transforms as

$$\Delta\mu_{\rm WBM}(T,C,\varphi)=\frac{RT_A}{v_m}\ln\frac{C^{T/T_A}}{C_l e^{[1-p(\varphi)]\Theta T/T_A}}. \quad \text{(C3)}$$

This expression can be compared with the chemical potential difference predicted by the EFKP model as is given in the following section.

### 2. Chemical potential difference for the EFKP model

From the definition of the chemical potential (17) and using the inner energy (A5) one can obtain the difference between potentials at a given temperature and in equilibrium:

$$\begin{aligned}\Delta\mu_{\rm EFKP}&\equiv\mu_{\rm EFKP}(T,C,\varphi)-\mu_{\rm EFKP}(T_A,C,\varphi)\\&=\epsilon(\varphi)-\epsilon_l+\frac{RT}{v_m}\ln C-\frac{RT_A}{v_m}\ln C_l\\&=\frac{\epsilon_s-\epsilon_l}{2}[1+p_\epsilon(\varphi)]+\frac{RT}{v_m}\ln C-\frac{RT_A}{v_m}\ln C_l.\end{aligned} \quad \text{(C4)}$$

As for the WBM model (see Appendix C 1), equilibrium liquid concentration $C=C_l$ with $\varphi=1$ is taken for the equilibrium potential $\mu_{\rm EFKP}(T_A,C,\varphi)$. Using the definition (7) for the $p_\epsilon(\varphi)$ function and taking the $\Theta$ function from Eqs. (40) and (C4)

can be rewritten in the following form:

$$\Delta\mu_{\mathrm{EFKP}} = \frac{RT_A}{v_m} \ln\left(\frac{C^{T/T_A}\Theta(\varphi)}{C_l(k_e-1)}\right), \tag{C5}$$

convenient for the further analysis. Particularly, with known profiles $C(x)$ and $\varphi(x)$ one can compute and compare spatial profiles of $\Delta\mu$ by Eqs. (C3) and (C5) for the obtained value of $T$, i.e., for a given interface velocity $V$.


[1] A. A. Chernov, in *Rost Kristallov*, edited by A. V. Shubnikov and N. N. Sheftal, Vol. 3 (Akademia Nauk SSSR, Moscow, 1959), p. 35 [English translation: *Growth of Crystals*, Vol. 3 (Consultants Bureau, New York, 1962), p. 65]; V. V. Voronkov and A. A. Chernov, Sov. Phys. Crystallogr. **12**, 186 (1967); A. A. Chernov, Usp. Fiz. Nauk **100**, 277 (1970) [Sov. Fiz. Usp. **13**, 101 (1970)].

[2] J. C. Baker and J. W. Cahn, Acta Metall. **17**, 575 (1969).

[3] M. J. Aziz, J. Appl. Phys. **53**, 1158 (1982).

[4] M. J. Aziz and T. Kaplan, Acta Metall. **36**, 2335 (1988).

[5] A. A. Wheeler, W. J. Boettinger, and G. B. McFadden, Phys. Rev. E **47**, 1893 (1993).

[6] M. Conti, Phys. Rev. E **56**, 3717 (1997).

[7] N. A. Ahmad, A. A. Wheeler, W. J. Boettinger, and G. B. McFadden, Phys. Rev. E **58**, 3436 (1998).

[8] K. Glasner, Physica D **151**, 253 (2001).

[9] D. Danilov and B. Nestler, Acta Mater. **54**, 4659 (2006).

[10] P. Galenko, Phys. Rev. E **76**, 031606 (2007).

[11] V. G. Lebedev, E. V. Abramova, D. A. Danilov, and P. K. Galenko, Int. J. Mater. Res. **101/04**, 473 (2010).

[12] D. Herlach, P. Galenko, and D. Holland-Moritz, *Metastable Solids from Undercooled Melts* (Elsevier, Amsterdam, 2007).

[13] Y. Yang, H. Humadi, D. Buta, B. B. Laird, D. Sun, J. J. Hoyt, and M. Asta, Phys. Rev. Lett. **107**, 025505 (2011).

[14] B. Echebarria, R. Folch, A. Karma, and M. Plapp, Phys. Rev. E **70**, 061604 (2004).

[15] P. Galenko and D. Jou, Phys. Rev. E **71**, 046125 (2005).

[16] V. Lebedev, A. Sysoeva, and P. K. Galenko, Phys. Rev. E **83**, 026705 (2011).

[17] A. A. Wheeler, W. J. Boettinger, and G. B. McFadden, Phys. Rev. A **45**, 7424 (1992); G. B. McFadden and A. A. Wheeler, Proc. R. Soc. London, Ser. A **458**, 1129 (2002); D. Danilov and B. Nestler, Discrete Contin. Dyn. Syst. **15**, 1035 (2006).

[18] J. Tiaden, B. Nestler, H. J. Diepers, and I. Steinbach, Physica D **115**, 73 (1998); D. A. Cogswell and W. C. Carter, Phys. Rev. E **83**, 061602 (2011).

[19] P. Galenko, Phys. Lett. A **287**, 190 (2001).

[20] The solute trapping phenomenon is studied in this work on the time scales of $\tau_D$. For most metallic and nonmetallic systems the inequality $\tau_\varphi \ll \tau_D$ holds [11]. Therefore investigations of the semihyperbolic phase-field model instead of fully hyperbolic model can be accepted as a reasonable approximation.

[21] D. Jou, J. Casas-Vazquez, and G. Lebon, *Extended Irreversible Thermodynamics*, 4th ed. (Springer, Berlin, 2010).

[22] M. Grmela and H. C. Ottinger, Phys. Rev. E **56**, 6620 (1997); M. Grmela, G. Lebon, and Ch. Dubois, *ibid.* **83**, 061134 (2011).

[23] P. K. Galenko and D. A. Danilov, J. Cryst. Growth **216**, 512 (2000).

[24] In principle, the $h(p,V)$ function can be arbitrarily chosen with the conditions of its monotonic behavior at any values of $V$ and its transforming into the preliminary chosen $h(p,V=0)$ function at equilibrium. The detailed form of the $h(p,V)$ function might also be optimized using the results of atomistic modeling (like the molecular dynamics simulations) or the results from modeling on the atomic lengths and diffusive time scales (like the phase-field crystal modeling).

[25] B. Vinet, L. Magnusson, H. Fredriksson, and P. J. Desre, J. Colloid Interface Sci. **255**, 363 (2002).

[26] J. A. Kittl, M. J. Aziz, D. P. Brunco, and M. O. Thompson, J. Cryst. Growth **148**, 172 (1995).

[27] V. T. Borisov, Dokl. Akad. Nauk SSSR **142**, 69 (1962) [Sov. Phys. Dokl. **7**, 50 (1962)].

[28] P. Galenko and S. Sobolev, Phys. Rev. E **55**, 343 (1997).